Fraunhofer Institut
Umwelt-, Sicherheits-,
Energietechnik UMSICHT

Inline Measurement Of Particle Size: Development Of a New Method

Master Thesis Report

By

Kamrul Islam

Accomplished on

March 2005

Supervised by

Dr. Jan Blömer

In co-operation with

Lehrstuhl für Technische Thermodynamik
Prof. Dr.-Ing. A. Leipertz
University of Erlangen-Nürnberg

PD Dr. Friedrich Dinkelacker

Contents

Chapter 1

Introduction

In-process or in-line particle analysis is key to optimising particulate processes and improving product quality and performance of grinding mill. No proven devices are currently available for in-line monitoring of particle size distribution. Available modern measuring methods based on laser diffraction or the coupling of digital camera technology and software-supported image analysis represent so far no optimal solution. Usually only one component current of the particle collective can be measured, whose portion with sinking particle size becomes ever smaller. As a result the representative sampling is not possible by the conventional method. In addition, most instruments which are commercially available were not designed for use in an industrial environment, where they are exposed to dust, heat and vibrations. Specially in case of cryogenic grinding process at the outlet of mill the temperature goes down to $-50\,^{\circ}\mathrm{C}$ and it is difficult to get optical access of particulate flow. Furthermore the investment costs are high. For the control of particulate process a simplified and robust sizing probe is required that provides one or more output signal (currents) that can be used as feedback signals for the aspects of the Particle Size Distribution (PSD) to be controlled. Improvements in process measuring and control are commonly driven by traditional goals of safety, cost control and the product quality. Enhancement of the process efficiency and control of product property related a demand for in-line real-time particle size measurements. The advantages in general are followings [7].

- Direct correlation between grinding conditions, powder properties and product quality. No time delay between sampling and analysis. Process conditions stored in database can serve as a tool for system analysis. Traceabilty of disturbances can lead to process improvements and better customer support.

- Real-time data aqusition, numerical processing and transmission of the measured signal to the digital control system of the grinding plant.

- Ability to detect process changes that are related to the aspect of PSD that are to be controlled. Absolute accuracy of the signal is not essential.

- Better statiscal basis for quality analysis as a result of the larger number of measurements that are continuously taken from a moving product flow. Further advantage are the exclusion of the operator effects and segregation problems on sampling without requiring an operator for continuous cleaning and calibration

Fraunhofer UMSICHT used optical measuring device manufactured by Parsum GmbH for in-line PSD measurement in order to use in the cryogenic grinding mill. The results were not representing of the mill product. Therefore, the objective of this thesis is to develop a new method of in-line particle sizing for control purpose by which representive sampling would be possible and the investment cost would be less.

In this thesis numerical calculations of particle-laden flow of the designed model was performed by using commercial CFD software FLUENT. Experimental system was developed and experiments were carried out to measure PSD in-line.

Chapter 2

In-line Particle Size Measurement

2.1 The Motivation For In-line Measurement

The particulate state of products in chemical industry is very important Large chemical companies such as BASF and DuPont found that more than 60% of their products were powders, crystalline solids, granules, dispersions, slurries and pastes [9]. A further 15% of the products incorporated particles to impart key end-use properties.

Grinding technique which is used to produce a fine powder with a narrow particle PSD from feed material. The PSD determines greatly the behaviour of the material in succeeding unit operations such as chemical reactions, combustion, printing or coating. The desired properties of a powder depend on the application. For instance, the reactivity or solubility of the product is usually related to the maximum surface area, which depends on the maximum the relative amount of the fines present in the powder. Complete conversion in combustion, chemical reaction and solution process are determined by maximum specific surface area of particles. Other characteristic affected by particle size are flowability and bulk density. For a smooth coating surface the top size of the paint/coating particle are critical. Furthermore, the brightness and colour of pigments are related to the whole PSD as a result of light diffraction. Other examples are the strength of cement and the taste of chocolate. Finally dust problems and explosion risk during handling can be controlled by proper PSD. The above examples illustrated how the product specification is often related to the PSD. This underlies the importance of an automated grinding plant equipped with a real-time PSD instruments for quality control. For control purposes an absolute accuracy of the produced PSD is not required. The real-time particle size monitoring of the process reduced the production of off-specification material. A simple feedback control based on in-line measurements allowed an operation of the mill that is closer to the specification limit, thus avoiding a considerable amount of off specification material.

2.2 Particle Size Distribution

2.2.1 Graphical Representation of Particle Size Distribution

A powder consists of a collection of particles with different size and shapes. The PSD describes the spectrum of sizes in powder sample. Two commonly used ways to represent the PSD are the density distribution and cumulative undersize distribution. Figures 2.1

Figure 2.1: Density distribution

Figure 2.2: Cumulative distribution

and 2.2 show typical size distribution of an industrial powder, which is usually considered to be a continuous curve.

Density Distribution

The particle size density distribution $q_r(x)$ of a powder expresses the amount of material present in each size class related to the amount of total sample.

Cumulative Distribution

The cumulative undersize distribution $Q_r(x)$describes the volume percentage of the powder that is finer than a specified size. The use of these curve is common in industrial practice as product specifications can easily and fast be compared.

$$Q_r(x) = \int_{x_{min}}^{x} q_r(x)dx \tag{2.1}$$

Discrete Size Vector

In practice it is convenient to depict PSD curves as a histrogram. Traditionally used sieves produce discretised results as do many of the modern devices, such as electrical resistance, light scattering or ultrasound instruments due to numerical processing.

2.2.2 Basis of Distribution

A physical property has to be chosen to characterise the size of particles. Particle size distribution $q_r(x)$ as fraction of the total sample are presented on different bases in terms of equivalent spheres. The PSD is called to be volume based (r=3) when it is expressed as the volume of particles present in each size class. When the surface area is of interest the PSD can be based on area per size class (r=2). The number of particles per size class is given by the number density (r=0). In the case of attrition the number of fines produced is very large, whilst the volume of these fractions will be low. With respect of thermodynamics it is interesting to look at the newly created surface area. Since in the population balance model the mass balances during the grinding process are to be

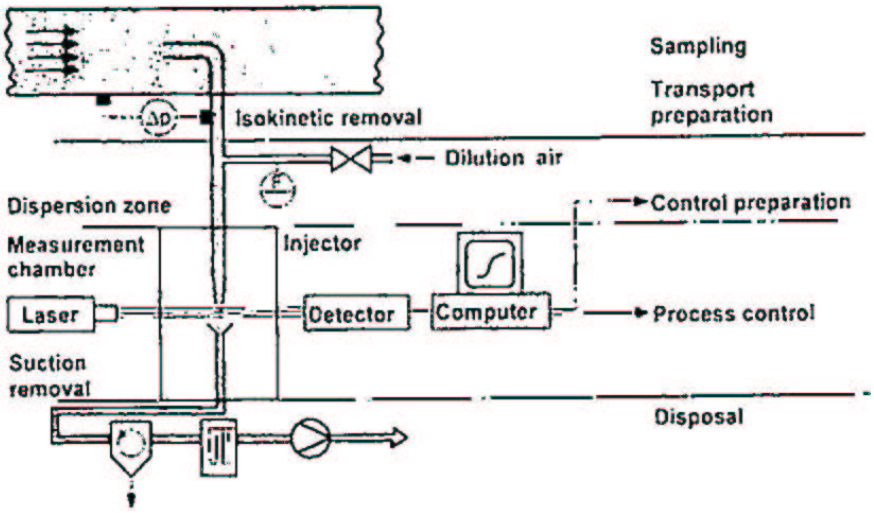

Figure 2.3: Online Measurement [9]

solved for each size class the volume diameter is most appropriate. So depending on the application a specific basis has to be chosen.

Particle Sizing Parameter

The modal size is the particle size at which the q_n(x) shows as a maximum. The median size, $x_{50}$is the 50% of the cumulative size distribution.

2.3 Particle Sizing Instruments

Over the last decade, a varities of technologies have been introduced for in-process particle sizing depending on applications. Meanwhile, applications have developed in the dryend (particles suspended in air) and wet-end (particle suspended in a liguid) areas. Here discussions have been focused on the dryend. Laser diffraction, Ultrasonics, focused beam reflectance measurement (FBRM), particle image analysis are most often used.

On-line Laser Diffraction

On-line measurements can be carried out under real process conditions involving sample taking (see Fig. 2.3). A measurement device that does not require sample taking and preparation is supposed to work in-line. Figure 2.3 shows the schematic view of the on-line measurement method based on laser diffraction. The sample is withdrawn from the pipeline and diluted with additional clean air in order to reach an appropiate obscuration level for instrument. This stream passes a laser beam wich is much wider than the particle size, leading to a scattering pattern of the ensample that is projected on to a photo detector. After signal processing size distribution is revealed. The problem of the method is representative sampling is not possible. While withdrawing sample the sample should be kept in the same condition as it was in the process. To keep the sample line clean and disposal of the sample are also tiresome.

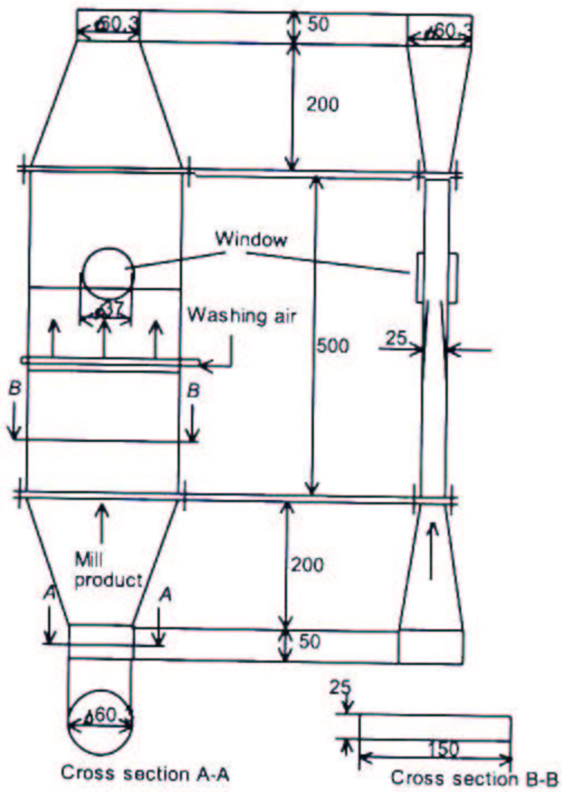

Figure 2.4: Inline sampling cell [7]

In-line sampling Cell

One in-line cell (see Fig. 2.4) together with laser diffraction instrument have been used. The most significant problem of the method has been found that particles can deposit on the windows of in-line cell. These particles would cause diffraction of the laser light and thus influence the signal value. In addition, it is not applicable for pipe of any diameter.

Imaging

This is a probe based high-resolution in-process video microscope that provides images of particles as they exist in a process. A charge couple device (CCD) camera is used to capture images of a particulate flow field, illuminated by a laser sheet. The particle size distribution is determined by processing the images.

FBRM

This is a probe based measurement tool that is installed in a pipeline. It uses a focus beam of laser light that scans in a circular path across a particle or particle stucture passing infront of the probe window. Upon hitting the particle, light is scattered in all directions. Light scattered back towards the probe is used to measure is used to measure a chord length (i. e. the length between any two points on a particle). Thousands of chords are measured per second. This mesurement is sensitive to the change in number, dimension or shape of particles under investigation.

Ultrasonics

Ultrasonic techniquiques are split into two areas: acoustic spectroscopy and electroacoustic spectroscopy. Acoustic spectroscopy is based on the scattering theory, which uses fundamental equation of mass, momentum and energy to describe the interaction between an ultrasonic wave and a suspended particle. The interaction of a particle and wave also depends on the frequency of the wave and the size of the particle. Therefore, if the fundamental equations and frequency are known, the size of the particle can be determined. On the other hand, elctroacoustic technique uses electric impulses to stimulate the particles, which then produce sound waves that are proportional to the particle size. Characterized by a wide measurement range, ultrasonic techniques can measure submicron-sized particle, and in some cases, be implemented non-invasively. In addition, ultrasonic technique typically require intricate knowledge about physical properties of the medium being measured including thermal conductivity, thermal expansion, heat capacity, shear rigidity/modulus (for solid phase), viscosity (for liquid phase) and intrinsic attenuation. In a dynamic particle system, it can be difficult to collect this information. Furthermore, the information can change overtime, making the acoustical techniques difficult to implement.

Chapter 3

New In-line Measurement Method

3.1 Concept of New Measurement Method

Measurement based on two modules

- Air classification
- Force sensing of different sized class particles by sensor

Air classification

Air classification is a process where different flow properties of particles (particle inertia, drag force acting on particle) of different sizes are exploited to achieve a separation based on particle size (aerodynamic diameter), shape or density. Most often size is used for separation. A quantity of material entering the system is separated by gradient of air flow into a size distribution. By exploiting these properties of particle when a impactor is introduced in the flow path of particulate process, different sized particles will strike at different radial position of impactor. For design and modeling of the device a detailed consideration of the mentioned relevant physical phenomena effecting the particle motion as for example turbulent transport of particles, particle wall interactions, particle-particle interaction is mandatory. In the following sections, the number of the relevant physical effects in dispersed two phase flows will be introduced and discussed.

Force sensing of different sized class particle by sensor

Measurements of dynamic oscillating forces and impact may require sensors with special capabilties. Different force sensors (piezo ceramic, quartz) are available to perform the measurement. When force is applied to this sensor, the sensor material generates an electric charge that is proportinal to the input force. Generated charges also depend on types of material. This charge output is collected on electrodes that are sandwiched between the materials. It is then either routed directly to an external charge amplifier or converter to a low impedence voltage signal within the sensor.

3.2 Theory of dispersed two phase flow

3.2.1 Parameter of dispersed flow

For the characterisation of dispersed two-phase flows different properties are used, which are briefly summarised below. The volume fraction of the dispersed phase is the volume occupied by the particles in a unit volume. Hence this property is given by

$$\alpha_p = \frac{\sum_i N_i V_{pi}}{V} \tag{3.1}$$

where N_i is the number of particles in the size fraction i, having the particle volume $V_{pi} = \frac{\pi}{6} D_{pi}$ The particle diameter D_{pi} in this context is the volume equivalent diameter of a sphere. Since the sum of the volume fraction of the dispersed phase and the continuous phase is unity, the continuous volume fraction is:

$$\alpha_F = (1 - \alpha_p) \tag{3.2}$$

The bulk density ρ_p^b or concentration c_p of the dispersed phase is the mass of particles per unit volume and hence given by:

$$\rho_p^b = c_p = \alpha_p \rho_p \tag{3.3}$$

Correspondingly, the bulk density of the continuous phase is:

$$\rho_F^b = (1 - \alpha_p)\rho_F \tag{3.4}$$

The sum of both bulk densities is called mixture density:

$$\rho_m = \rho_F^b \rho_p^b = (1 - \alpha_p)\rho_F + \alpha_p \rho_p \tag{3.5}$$

Often the particle concentration is also expressed by the number of particles per unit volume, as for example in clean-room technology. Especially in gas-solid flows the mass loading is frequently used, which is defined as the mass flux of the dispersed phase to that of the fluid:

$$\eta = \frac{m_p}{m_F} = \frac{\rho_p \alpha_p U_p}{(1 - \alpha_p)\rho_F U_F} \tag{3.6}$$

The proximity of particles in a two-phase flow system may be estimated from the inter-particle spacing, which however can be only determined for regular arrangements of the particles. For a cubic arrangement the inter-particle spacing (the distance between the centres of particles) is obtained from:

$$\frac{L}{D_p} = \left(\frac{\pi}{6\alpha_p}\right)^{\frac{1}{3}} \tag{3.7}$$

For a volume fraction of 1 % the spacing is 3.74 diameters and for 10 % only 1.74. Hence, for such high volume fractions the particles cannot be treated to move isolated, since fluid dynamic interactions become of importance. In many practical fluid-particle systems however, the particle volume fraction is much lower. Consider for example a gas-solid flow (particle density ρ_p= 2500 kg/m^3, gas density of ρ_F = 1.18 kg/m^3) with a mass loading of one then the volume fraction is about 0.05% (i. e. $\alpha_p = 5 \cdot 10^{-4}$). This results in an inter-particle spacing of about 10 particle diameters, hence, under such a condition a fluid dynamic interaction may be neglected.

A classification of dispersed two-phase flows with regard to the importance of interaction mechanisms was provided by Elghobashi [3]. Generally it is separated between dilute and dense two-phase flows.

- dilute dispersed two phase flow

$$\eta < 1, \alpha_p < 10^{-3} \tag{3.8}$$

- dense dispersed two phase flow

$$\eta > 1, \alpha_p > 10^{-3} \tag{3.9}$$

A two-phase system may be regarded as dilute for volume fractions up to $\alpha_p = 10^{-3}$ ($L/D_p \approx 8$). In this regime the influence of the particle phase on the fluid flow may be neglected for $\alpha_p < 10^{-6}$ ($L/D_p \approx 80$). For higher volume fractions the influence of the particles on the fluid flow, which is often referred to as two-way coupling, needs to be accounted for. In the dense regime (for $\alpha_p > 10^{-3}$) additionally interparticle interactions (collisions and fluid dynamic interactions between particles) become of importance.

3.2.2 Particle motion in fluids

The motion of particles in fluids is described in a Lagrangian way by solving a set of ordinary differential equations along the trajectory in order to calculate the change of particle location and the linear and angular components of the particle velocity. This requires the consideration of all relevant forces acting on the particle. The equation of motion for small particles in a viscous quiescent fluid (for small particle Reynolds-numbers, which is also referred to as Stokes flow) goes back to the pioneering work of Basset, Boussinesq and Oseen. Therefore, the equation of motion is mostly referred to as BBO-equation. Numerous publications deal with the extension of the BBO equation for turbulent flows. The thesis of Tchen was probably the first study on particle motion in turbulent flows based on the BBO equation [2]. A rigorous derivation of the equation of motion for small particles in non-uniform flow has been performed by Maxey and Riley [2]. Neglecting the Faxen terms the equation proposed by Maxey and Riley for small particle Reynolds numbers is as follows:

$$\begin{aligned} m_p \frac{d\vec{u}_p}{dt} &= \frac{18\mu_F}{\rho_p D_p^2} m_p(\vec{u}_F - \vec{u}_p) - m_F \frac{D\vec{u}_F}{Dt} + 0.5 m_F\left(\frac{D\vec{u}_F}{Dt} - \frac{d\vec{u}_p}{dt}\right) \\ &\quad + 9\sqrt{\frac{\rho_F \mu_F}{\pi}} \frac{m_p}{\rho_p D_p} \int_0^t \frac{\frac{D\vec{u}_F}{D\tau} - \frac{d\vec{u}_p}{d\tau}}{(t-\tau)^1/2} d\tau + (m_p - m_F)\vec{g} \end{aligned} \tag{3.10}$$

Considering spherical particles and neglecting heat and mass transfer phenomena, the calculation of particle trajectories requires the solution of three ordinary differential equations when particle rotation is accounted for. Hence, the differential equations for calculating the particle location, and the linear and angular velocities in vector form are given by:

$$\frac{d\vec{x}_p}{dt} = \vec{u}_p \tag{3.11}$$

$$m_p \frac{d\vec{u}_p}{dt} = \sum \vec{F}_i \tag{3.12}$$

$$I_p \frac{d\vec{\omega}_p}{dt} = \vec{T} \tag{3.13}$$

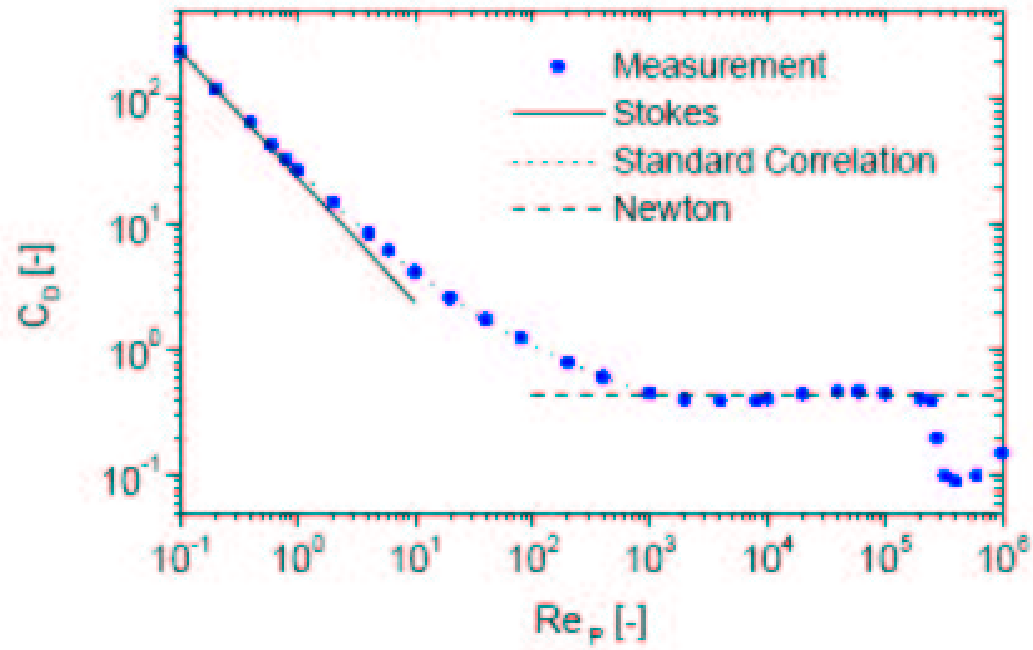

Figure 3.1: Drag coefficient as a function of particle Reynolds number [19]

Where $m_p = \pi/6 \rho_p D_p^3$ is the particle mass and $\vec{F}_i$ different relevant forces acting on the particle. Analytical solutions for the different forces only are available for small particle Reynolds numbers (Stokes regime). An extension to higher Reynolds numbers is generally based on empirical correlations which are derived from experiments.

Drag Force

In most fluid-particle systems the drag force is dominating the particle motion and consists of a friction and form drag. The extension of the drag force to higher particle Reynolds numbers is based on the introduction of a drag coefficient C_D being defined as:

$$C_D = \frac{\vec{F}_D}{\frac{\rho_F}{2}(\vec{u}_F - \vec{u}_p)^2 A_p} \tag{3.14}$$

Where $A_p = \pi/4 D_p^2$ is the cross section of the spherical particle. The drag force is expressed by:

$$\vec{F}_D = \frac{3}{4}\frac{\rho_F m_p}{\rho_p D_p} c_D(\vec{u}_F - \vec{u}_p) \mid \vec{u}_F - \vec{u}_p \mid \tag{3.15}$$

The drag coefficient C_D is given as a function of the particle Reynolds number:

$$Re_p = \frac{\rho_F D_p(\vec{u}_F - \vec{u}_p)}{\mu F} \tag{3.16}$$

The dependence of the drag coefficient of a sphere (spherical particle) on the Reynolds number is shown graphically based on numerous experimental investigations [19]. From this dependence one may identify several regimes which are associated with the flow characteristics around the sphere:

- For small Reynolds numbers ($Re_p < 0.5$) viscous effects are dominating and no separation is observed. Therefore, an analytic solution for the drag coefficient is possible as proposed by Stokes:
$$C_D = \frac{24}{Re_p} \tag{3.17}$$
This regime is often referred to as the Stokes-regime.

- In the transition region ($0.5 < Re_p < 1000$) inertial effects become of increasing importance. Above a Reynolds number of about 24 the flow around the particle begins to separate. Initially this separation is symmetric [2]. It becomes unstable and periodic above $Re_p \approx 130$. For this non-linear regime numerous correlations have been proposed which fit the experimental data more or less accurate. A frequently used correlation is that proposed by Schiller and Naumann [2], which fits the data up to $Re_p = 1000$ reasonably well.
$$C_D = \frac{24}{Re_p}(1 + 0.15{Re_p}^{0.687}) \tag{3.18}$$

- Above $Re_p \approx 1000$ the drag coefficient remains almost constant up to the critical Reynolds number, since the wake size and structure are not considerably changing. This regime is referred to as Newton-regime with:
$$C_D \approx 0.44 \tag{3.19}$$

- At the critical Reynolds number ($Re_{crit} = 2.5 \cdot 10^5$) a drastic decrease of the drag coefficient is observed, being caused by the transition from a laminar to a turbulent boundary layer around the particle. This results in a decrease of the particle wake.

- In the super-critical region ($Re_p > 4.0 \cdot 10^5$) the drag coefficient again increases continuously. For most practical particulate flows however this region is not relevant.

The drag coefficient may be altered by numerous other physical effects, such as turbulence of the flow, surface roughness of the particle, particle shape, wall effects, compressibility of the fluid, rarefaction effects, which in general can be only accounted for by empirical correction factors or functions being derived from detailed experiments. The turbulence level of the ambient flow essentially causes a reduction of the critical Reynolds number as shown by Torobin and Gauvin [2]. With increasing turbulence intensity the transition from laminar to turbulent boundary layer is shifted towards smaller particle Reynolds numbers. A surface roughness on a spherical particle also results in a reduction of the critical Reynolds number [2]. The consideration of the particle shape in the calculation of particle motion is rather difficult, since it requires actually the solution of additional ordinary differential equations for the particle orientation and a projection of the forces with regard to the relative motion. Such an approach was recently introduced by Rosendahl [18]. Therefore, most compuations rely on the assumption of spherical particles. A simplified approach to consider a non-sphericity of the particle may be based on the use of modified drag coefficients, which are provided for different non-spherical particles for example by Haider and Levenspiel [8]. It is however very little known about particle shape effects in the other forces, such as added mass and transverse lift forces. The motion of particles in the vicinity of a rigid wall results in an increase of the drag coefficient and is additionally associated with a transverse lift force. Analytic solutions for the wall effect are again only available for very small particle Reynolds numbers. The particle motion normal to a wall was for example considered by Brenner [2] and a wall-parallel motion was analysed by Goldman et al. [2]. The first order solution for a particle moving towards a wall, which is valid for large distances from the wall, is given by Brenner. Rarefaction effects become of importance in a low pressure environment or when the particles are very small. In such a situation the gas flow around the particle cannot be regarded as a continuum, instead the particle motion is induced by collisions of gas molecules with the particle surface. This results in a reduction of the drag coefficient. The importance of rarefaction effects may be estimated based on the ratio of the mean free path of the gas molecules to the particle diameter, which is the particle Knudsen number. A classification of the different flow regimes in rarefied conditions or for very small particles may be based on the Knudsen number Kn_p which is calculated by kinetic theory of gases. In the Stokes regime which is generally valid for very small particles, the reduction of the drag coefficient may be accounted for by a correction function, the so-called Cunningham correction, resulting in a modified drag [2]:

$$C_D = \frac{C_{D,stokes}}{Cu} \tag{3.20}$$

This correlation is valid for $0.1 < Kn_p < 1000$ and $Re_p < 0.25$ and is only applicable for low particle Mach numbers. Therefore, it is often used in particle technology, as for example when considering the separation of fine particles from a gas. The Cunningham correction (1/Cu) is plotted in Fig. 3.2 as a function of the Knudsen number. It is obvious, that a considerable reduction of the drag coefficient occurs for $Kn_p > 0.015$. The compressibility of the fluid becomes of importance when the relative velocity becomes so large that the particle Mach number increases beyond 0.3. In such a situation compression waves or even shock waves (for $Ma_p > 1$) are initiated by the particle motion which cause an increase of the drag for large particle Reynolds numbers. The particle Mach number is defined as:

$$Ma_p = \frac{\mid \vec{u}_F - \vec{u}_p \mid}{a} \tag{3.21}$$

where a is the speed of sound given by:

$$a = \sqrt{\gamma R T} \tag{3.22}$$

In Eq. 3.22 γ is the ratio of the specific heats, R is the universal gas constant, and T the absolute temperature of the gas. Numerous correlations, which are mostly based on experimental studies, are proposed to account for compressibility effects, as for example expression proposed by Carlson and Hoglund [2] which concluded for small particles the drag coefficient is decreasing due to rarefaction effects, whereas it increases for large particles beyond a Mach number of about 0.6 due to compressibility effects. Other expressions for the drag coefficient including rarefaction and compressibility effects are given by Crowe et al. [2]. The detail theory of drag force is described in literature [19].

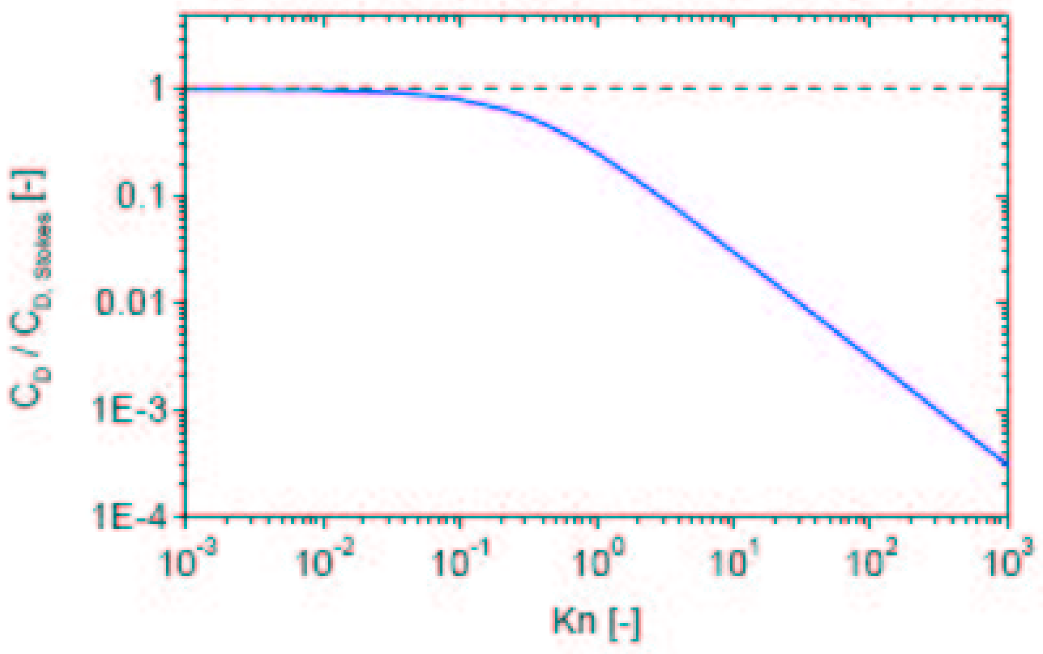

Figure 3.2: Drag coefficient during rarefaction effects [2]

Body Forces

Body forces are the gravity force, the Coulomb force, which arises when a particle moves in an electric field, as for example in an electrostatic precipitator or the thermophoretic force which becomes of importance when a small particle moves in a flow with a high temperature gradient. The gravity force is:

$$\vec{F}_g = m_p \vec{g} \tag{3.23}$$

Pressure Gradient and Buoyancy Force

The local pressure gradient in the flow gives rise to an additional force in the direction of the pressure gradient. Combining the pressure gradient with the shear stress in the fluid, one obtains:

$$\vec{F}_p = \frac{m_p}{\rho p}(-\nabla p + \nabla \tau) \tag{3.24}$$

From the Navier-Stokes equation of the fluid the pressure gradient and the shear stress can be related to the fluid acceleration and the gravity force:

$$-\nabla p + \nabla \tau = \rho_F (\frac{D\vec{u}_F}{Dt} - \vec{g}) \tag{3.25}$$

Hence the total pressure force is obtained in the following form:

$$\vec{F}_p = m_p \frac{\rho F}{\rho p} (\frac{D\vec{u}_F}{Dt} - \vec{g}) \tag{3.26}$$

The first term of Eq. 3.26 represents the fluid acceleration and the second one is the buoyancy force. It is obvious, that in gas solid flows the pressure force may be neglected since $\rho_F/\rho_p << 1$. However, in liquid solid flows this force is of importance since $\rho_F/\rho_p \approx 1$.

Added Mass and Basset Force

The acceleration/deceleration of a particle in a fluid also requires to accelerate/decelerate a certain fraction of the surrounding fluid, this is the so-called added mass. The Basset force is caused by the lagging of the boundary layer development on the particle with changing relative velocity (acceleration or deceleration of the particle) and is often referred to as history force.

Slip-Shear Lift Force

Particles moving in a shear layer experience a transverse lift force due to the non-uniform relative velocity over the particle and the resulting non-uniform pressure distribution. The lift force is acting towards the direction of higher slip velocity. An expression for the slip shear lift force for a freely rotating particle moving at constant velocity in a twodimensional shear flow at low Reynolds number was derived from an asymptotic expansion by Saffman [2].

Slip-Rotation Lift Force

Particles which are not freely rotating in a flow may also experience a lift force due to their rotation, the so-called Magnus force. High particle rotations may for example be induced by particle-wall collision frequently occurring in pipe or channel flows. The rotation of the particle results in a deformation of the flow field around the particle, associated with a shift of the stagnation points and a transverse lift force. An analytic expression for the slip-rotation lift force in the case of small particle Reynolds numbers was derived by Rubinow and Keller. Also the slip-rotation lift force may be extended for higher particle Reynolds numbers by modification of the previous equation [2].

Response Time and Stokes Number

The particle (velocity or momentum) response time may be used to characterise the capability of particles to follow a sudden velocity change in the flow, occurring for example in large scale vertical structures or turbulent eddies. In order to derive the particle response time the equation of motion is used by only considering the drag force.

$$m_p \frac{d\vec{u}_p}{dt} = \frac{\rho_F}{2} \frac{\pi}{4} {D_p}^2 C_D \mid \vec{u}_F - \vec{u}_p \mid (\vec{u}_F - \vec{u}_p) \tag{3.27}$$

Dividing by the particle mass and introducing the particle Reynolds number gives:

$$\frac{d\vec{u}_p}{dt} = \frac{18\mu_F}{\rho_p D_p^2} \frac{C_D Re_p}{24} (\vec{u}_F - \vec{u}_p) \tag{3.28}$$

The term $C_D Re_p/24$ corresponds to the non-linear term in the drag coefficient f_D and the first term of Eq. 3.29 has the dimension of a time, the particle response time:

$$\tau_p = \frac{\rho_p D_p^2}{18\mu_F f_D} \tag{3.29}$$

Hence the equation of motion becomes:

$$\frac{d\vec{u}_p}{dt} = \frac{1}{\tau_p}(\vec{u}_F - \vec{u}_p) \tag{3.30}$$

The solution of this equation for a simplified case, namely a constant fluid velocity u_F and an initial particle velocity of zero is:

$$u_p = u_F\big(1 - exp\big(-\frac{t}{\tau_p}\big)\big) \tag{3.31}$$

From this equation it is obvious that τ_p is the time required for a particle released with zero velocity into a flow with u_F to reach 63.2 % of the flow velocity. In the Stokes-regime the particle response time Eq. 3.29 becomes:

$$\tau_p = \frac{\rho_p D_p^2}{18\mu_F} \tag{3.32}$$

since f_D approaches unity. The Stokes number is the ratio of the particle response time to a characteristic time scale of the flow.

$$St = \frac{\tau_p}{\tau_F} \tag{3.33}$$

More detail theory of particle flow in fluid is described in literature [2].

3.2.3 Particle Wall Collision

Particle-wall collisions become of importance in confined flows, such as pneumatic conveying or particle separation in cyclones. In pneumatic conveying, for example, the momentum loss of a particle caused by an inelastic wall impact is associated with a reacceleration of the particle after rebound. Hence, momentum is extracted from the fluid phase for this acceleration, causing an additional pressure loss. This pressure loss depends on the average wall collision frequency or mean free path between subsequent particle-wall collisions. The wall collision frequency is mainly determined by the following parameters:

- particle mass loading
- dimensions of the confinement, e. g. pipe diameter in pneumatic conveying
- particle response time or response distance
- conveying velocity and turbulence intensity
- particle shape and wall roughness
- combination of particle and wall material.

A first estimate of the importance of particle-wall collisions may be based on the ratio of the particle response distance λ_p to the dimension of the confinement, e. g. the diameter of the pipe D. The particle response distance can be estimated from the following equation [12].

$$\lambda_p = \frac{\rho_p D_p^2}{18 \mu_F f_D} \cdot w_t \tag{3.34}$$

where w_t is the terminal velocity of the particle. For the case λ_p is larger than the dimension of the confinement D, the particles are not able to respond to the flow, before they collide with the opposite wall, hence their motion is dominated by wall collisions. In addition to the above mentioned effects the wall collision process may be affected by hydrodynamic interaction which eventually causes a deceleration of the particle before impact. This effect however is only of importance for viscous fluids and hence small particle Reynolds numbers.

Velocity Change During Wall Collisions

Different models are established for particle wall collision. Hard sphere model for the wall collision implies a negligible particle deformation during the impact process. Moreover, Coulombs law of friction is assumed to hold for a sliding collision. For an inelastic collision process, one may identify a compression and a recovery period. The change of the particles translational and rotational velocities during the bouncing process can be calculated from the momentum equations of classical mechanics [2]. In short, the type of collision is determined by the static coeefficient of friction, the restitution ratio of normal velocity component and the velocity of the particle surface relative to the contact point. These parameters are not only dependent on the material of particle and wall but also on impact velocity and angle [12, 21].

Wall Roughness Effects

Several experimental studies have shown that wall roughness has a considerable impact on the particle wall collision process [11, 12]. In industrial processes, as for example pneumatic conveying, steel pipes are used, which have a mean roughness height between about 20 and 50 μm. Experimental studies of Sommerfeld and Huber [12] revealed, that the roughness angle distribution may be represented by a normal distribution function. The standard deviation of this distribution is influenced by the roughness structure and the particle size. The dimensions of the roughness structure suggest, that the wall collision process of small particles ($< 100 \mu m$) should be strongly affected, since they will be able to experience the details of the roughness structure. However, after rebound they will quickly adjust to the flow, so that the influence of the wall roughness effect is limited to the near wall region and will not strongly affect the particle behaviour in the bulk of the flow. On the other hand large particles may cover several roughness structures during wall impact. This implies that they feel less wall roughness. However, due to their high inertia, they will need more time to adjust to the flow after rebound. This eventually causes the wall roughness to be more important for the bulk behaviour of larger particles in a given flow [11]. In addition, the so-called shadow effect for small impact angles results in a shift of the effective roughness angle distribution towards positive values, since the particles are not able to reach the lee-side of the roughness structures. Hence, for small impact angles the effective impact angle is increased compared to the particle trajectory angle with respect to the plane wall [12]. This implies a transfer of momentum from the wall-parallel component to the normal component, i. e. the normal component of the rebound velocity becomes larger than the impact component. In pneumatic conveying this effect causes a re-dispersion of the particles, whereby the influence of gravitational settling is reduced [11].

3.2.4 Inter Particle Collision

Inter-particle collisions may have several consequences in particle-laden flows, such as heat and momentum transfer between particles, dispersion of regions with locally high particle concentration and eventually also agglomeration of particles. Essential for inter-particle collisions to occur is a relative motion between the particles. Such a relative motion may be caused by several mechanisms:

- Brownian or thermal motion of particles
- laminar or turbulent fluid shear
- particle inertia in turbulent flow
- mean drift between particles of different size (so-called differential sedimentation)

The collision rate (collisions per unit volume and time) between two particle fractions for above mentioned mechanisms have been described in literature. In turbulent flows the particle response and the importance of inter-particle collisions may be characterised by a turbulent Stokes number, which is the ratio of the particle response time τ_p to the relevant time scale of turbulence T_t:

$$St = \frac{\tau_p}{T_t} \tag{3.35}$$

Based on the Stokes number the limiting cases for the collision rate due to turbulence may be identified. For very small particles which completely follow turbulence ($St_t \rightarrow 0$) the expression of Saffman and Turner [2]. The other limiting case is the kinetic theory for ($St \rightarrow \infty$), where the particle motion is completely de-correlated with the fluid and hence the velocity of colliding particles is also de-correlated (granular medium). This case was analysed by Abrahamson [2] for heavy particles in high intensity turbulence neglecting external forces, which implies that there is no mean relative velocity between the particles. In practiculate two-phase flows the two limits (particles completely following turbulence ($St_t \rightarrow 0$) and heavy particles ($St \rightarrow \infty$)) are rarely met, rather the particles may partially respond to turbulence.

Importance of Inter-Particle Collisions

In the following the importance of inter-particle collisions in turbulent fluid-particle flows is discussed. The inter-particle collision probability depends mainly on the particle concentration, the particle size, and the fluctuating motion of the particles. A classification of particle-laden flows in terms of the importance of inter-particle collisions and the boundary between dilute and dense systems may be based on the ratio of particle response time τ_p to the averaged time between collisions τ_c. In dilute two-phase flows the particle motion will be mainly governed by fluid dynamic transport effects, i.e. drag force, lift forces, and turbulence. On the other hand dense flows are characterised by high collision frequencies between particles and hence their motion is dominantly influenced by inter-particle collisions. Fluid dynamic transport effects are of minor importance. Therefore, the two regimes are characterised by the following time scale ratios:

- dilute two-phase flow:

$$\frac{\tau_p}{\tau_c} < 1$$

- dense two-phase flow:

$$\frac{\tau_p}{\tau_c} > 1$$

This implies, that in dense two-phase flows the time between particle-particle collisions is smaller than the particle response time, whereby the particles are not able to completely respond to the fluid flow between successive collisions. This regime may occur when either very large particles at a low number density are present in the flow or in the case of small particles when the number density is large. In dilute two-phase flows collisions between particles may also occur and influence the flow development to a certain degree, but the time between successive inter-particle collisions is larger than the particle response time, whereby the fluid dynamic transport of the particles is the dominant transport effect. In the following section an estimate of the boundary between the two regimes will be given for turbulent particle-laden flows. The average time between successive inter-particle collisions results from the average collision frequency:

$$\tau_c = \frac{1}{f_c}$$

The collision frequency of one particle (i. e. $n_i = 1$) with diameter D_i and velocity u_i with all other particle classes (i. e. N_{class}) with diameter D_j and velocity u_j can be calculated according to kinetic theory of gases from:

$$f_c = \frac{N_{ij}}{n_i} = \sum_{j=1}^{N_{class}} \frac{\Pi}{4}(D_i + D_j)^2 \mid \vec{u}_i - \vec{u}_j \mid n_j \tag{3.39}$$

Modeling of inter-particle collisions in the frame of the the Euler/Lagrange method for numerical calculation of two phase flows has been based mainly on two approaches, a direct simulation and a model based on concept of kinetic theory of gases. The most straight forward method to account for inter-particle collision is the direct simulation method. A stochastic inter- particle collision model has been developed by Oestele and Petijean, Sommerfeld and Zivkovic [20]. Another model have been introduced by Eskin and Kalman [5].

3.2.5 Methods for the Prediction of Multiphase Flows

Over the last decade Computational Fluid Dynamics (CFD) is increasingly used by chemical industry for process analysis and optimisation. Most of these processes involve single- or multi-phase flows in complex geometries which may be also accompanied by heat and mass transfer and chemical reactions. Numerical computations of multiphase flows may be performed on different levels of complexity related to the resolution of the interface between the phases and the turbulence modelling:

- Direct Numerical Simulations (DNS) of particulate flows by accounting for the finite dimensions of the particles and the flow around the particles have become feasible in the part couple of years due to the drastic increase of computational power. Such an approach the timedependent solution of the three-dimensional Navier-Stokes equations on a grid resolves the particles. Two approaches are mainly being used to resolve the particle contour and respect the appropriate boundary condition at the surface. An adaptive unstructured grid is used in order to follow the particle motion and resolve the particle shape [10]. In the second approach the flow field is calculated on a regular grid and a tracer particle method (a template) is used to emulate the rigid particle. These kind of methods have been applied to flows with low particle Reynolds number, e.g. to calculated particle sedimentation processes.

- DNS as described above are also being applied to dispersed turbulent two-phase flows by considering the particles as point-particles and using the Lagrangian approach to simulate the dispersed phase. This implies that a large number of particles are simultaneously tracked through the computed time-dependent flow field by considering the relevant forces. This type of DNS has been applied mainly to basic turbulence research, in order to analyse the particle behaviour in turbulent flows and the effect of particle on turbulence [4].

- Large eddy simulations combined with the Lagrangian tracking of point-particles have been also applied to the study of basic phenomena in dispersed particulate flows, such as, particle dispersion in turbulent flows, inter-particle collisions [15]. The results are mainly used to derive and validate models and also to develop closures for the two-fluid approach.

- For engineering problems two approaches based on the Reynolds-averaged Navier-Stokes equations are commonly applied, namely the two-fluid or Euler/Euler approach and the Euler/Lagrange method. In order to account for the interaction between phases, i. e. momentum exchange and heat an mass transfer, the conservation equations have to be extended by appropriate source/sink terms.

In the two-fluid approach both phases are considered as interacting continua. Hence, properties such as the mass of particles per unit volume are considered as a continuous property and the particle velocity is the averaged velocity over an averaging volume (computational cell). Also the interfacial transfer of mass, momentum, or energy requires averaging over the computational cells. Especially in turbulent flows the closure of the dispersed phase Reynolds-stresses and the fluid-particle interaction terms are associated with sophisticated modelling approaches [17]. The consideration of a particle size distribution requires the solution of a set of basic equations for each size class to be considered. Hence the computational effort increases with the number of size classes. The Euler/Lagrange approach is only applicable to dispersed two-phase flows and accounts for the discrete nature of the individual particles. The dispersed phase is modelled by tracking a large number of particles through the flow field in solving the equations of motion taking into account the relevant forces acting on the particle. Generally, the particles are considered as point-particles, i.e. the finite dimension of the particles is not considered and the flow around the individual particles is not resolved. Since the number of real particles in a flow system is usually too large for allowing a tracking of all particles, the trajectories of computational particles (parcels) which represent a number of real particles with the same properties (i.e. size, velocity and temperature) are calculated. In stationary flows a sequential tracking of the parcels may be adopted, while in unsteady flows all parcels need to be tracked simultaneously on the same time level. Local average properties such as dispersed phase density and velocity are obtained by ensemble averaging. Statistically reliable results for each computational cell require the tracking of typically between 10,000 and 100,000 parcels, depending on the considered flow. The advantage of this method is that physical effects influencing the particle motion, such as particle-turbulence interaction, particle-wall collisions, and collisions between particles can be modelled on the basis of physical principles. Moreover, a particle size distribution may be easily considered by sampling the size of the injected particles from a given distribution function. Problems however may be encountered in the convergence behaviour for high particle concentration due to the influence of the dispersed phase on the fluid flow (two-way coupling) which is accounted for by source terms obtained through averaging particle trajectories [14]. Essential for a reliable application of both methods is the appropriate modelling of the relevant physical mechanisms affecting the particle motion, as for example, turbulent transport of particles, wall interactions of particles, collisions between particles and agglomeration. In some cases the physical phenomena are far too complicated to allow for a derivation of the model from basic principles of physics. Therefore, detailed experiments are required to analyse the considered phenomena and to derive appropriate empirical or semi-empirical models. In order to validate the models, the results of the numerical predictions need to be compared with bench mark test cases featuring the considered phenomena.

Chapter 4

CFD modeling

This chapter contains a study into the flow patterns of the measurement device and particle trajectory inside the device using computational fluid dynamics (CFD). The flow patterns of the device are important with respect to the classification of particles. As principle of the measurement method based on particle trajectories, it is very important to know the particle trajectories. In order to investigate two phase flow most often experiments is used which is time consuming, expensive and have many practical limitations. Considering all these limitations computational studies of this system was chosen. In this thesis the CFD software Fluent version 6.1.22 was used as a tool to carry out flow simulations and to calculate particle trajectories.

CFD

CFD software describes the fluid flow and heat transfer by solving the conservation equations for mass, momentum and energy. These partial differential equations are to be solved for geometries which are divided into a large number of small grid elements. The numerical solution progresses in time and space and finally should converge to a numerical description of the complete flow field in the machine that is modelled.

4.1 Definition of physical models

The flow at mill outlet is dispersed two phase flow. This section deals with the properties of the media and model used for the simulation.

Material properties

For the air standard viscosity and density was used. The density of solid material was 1200 kg per cubic meter, other properties of the material will be discussed in the following chapter.

Turbulence model

CFD software normally contain turbulence models which are approximations of the real physics. In order to close the equations and predicting correctly the turbulence quantities, Reynolds Stress Model (RSM) is applied. The use of RSM requires values for the turbulence intensity and characteristic length to set up the set of conservation equations. For the simulations a turbulence intensity of 5% at inlet and 1% at outlet was used, while the characteristic length was put equal to the diameter of the pipe inlet.

Solution control

Numerical simulations are performed on 2D domain. The spatial discretiztion of variable employed the following schemes: second order upwind differencing scheme for RSM, second order for pressure, second order for momentum, method SIMPLE for pressure velocity coupling.

Particle tracking

The dispersed phase is solved by tracking a large number of particles through the calculated flow field. The coupling between continuous and discrete phase (momentum, mass and energy exchange) and its impact on both the discrete phase trajectories and continuous phase flow has been included. Calculation of the discrete phase trajectory using a Lagrangian formulation that includes particle motion in fluid as described in Sec. 3.2.2 and [13]. The forces considered to act on the particle was discrete phase inertia, hydrodynamic drag and gravity force. The stochastic tracking model was used to include the dispersion of particles due to turbulence in the fluid phase. The stochastic tracking (random walk) model [13] includes the effect of instantaneous turbulent velocity fluctuations on the particle trajectories through the use of stochastic methods. A fundamental assumption made in this model is that the dispersed second phase occupied a low volume fraction, less than 12 volume percent. This assumption implies that the motion of particles is controlled by local dynamic forces. It was assumed that there is no particle interaction. The assumption is valid for the cases of this thesis where particle mass loading η (Eq.3.6) goes to maximum value of 0.2 where fluid dynamic transport of the particles is the dominant transport effect (see section 3.2.4). For particle tracking surface injection at system inlet is used. The solid mass flow rate at each radial position is distributed between the 10 different particle size classes according to Rosin-Rammler distribution [13]. The Rosin-Rammler distribution defines the mass fraction of particle sizes according to the following equations:

$$m_p = exp\Big(-(\frac{d_p}{\bar{d}_p})^n\Big) \tag{4.1}$$

where m_p is the mass fraction of particles with diameter greater than d_p, $\bar{d}_p$ is the mean volume diameter and n is the spread parameter. Spherical particle is considered for drag calculation. Rebounds the particle off the boundary in question with a change in its momentum as defined by the coefficient of restitution e. This is of two type: normal and tangential. The normal coefficient of restitution defines the amount of momentum in the direction normal to wall that is retained by the particle after collision with the boundary.

$$e = \frac{V_2}{V_1} \tag{4.2}$$

Where V is the particle velocity and the supscripts 1 and 2 refer to before and after collision. Normal or tangential $e = 1$ implies that particle retains all of its normal or tangential momentum after the rebound while $e = 0$ implies that the particle retains none of its normal or tangential momentum after the rebound.

All important boundary values that were used for all performed simulations are given in table 4.1.

Name	Value
Inlet gas velocity	$1 - 43\ m/s$
Inlet velocity of particles	$0.5 - 35\ m/s$
Distribution of particle size	$50 - 700\ \mu m$
Mass loading η	$0.03 - 0.2$
Mean particle size	$212\ \mu m$
Spread parameter of RR-distribution	6.1
Particle wall boundary condition : reflect with coefficient of restitution	0.1 (exception is mentioned with results)

Table 4.1: Values of boundary conditions

4.2 Simulated Models

The objective of the modeling was to find out a model which can classify feed particles of given particle size distribution in order to measure the particle size in line. There are many models which is used by the process industry or researcher to classify the final product by air flow called as air classifyer. Air classifyer commonly use to classify below 100 micron particles while particles used for this thesis are 50-700 micron. Brief description of these models (cyclone separator, cross flow separator, inertia separator etc.) are available in almost all particle technology books [1]. As the objective of this thesis is not classify particles but to measure PSD in-line. But for measurement of PSD air classification principle is used. The basic concept of some of those designs have been chosen for the the modeling of this thesis. Following models were simulated in this thesis.

Elbow model

Figure 4.1 shows 90 degree elbow of 100 mm diameter where 83196 triangular computatinal cells have been used for calculation. Particle tracking have been performed and particle classification was observed after rebouncing off wall where biggest particle follow longest path because of its higher momentum. This means that particle wall collision is the dominating separation parameter while gravity settling does not have effect in this case. Result also shows that smallest particle followed flow path as well as turbulence ($St_t \rightarrow 0$) to some extend and ultimately follow the flow path after entering to the system where as bigger particles do not follow. So the trajectory of bigger particles are straight.

Cross flow model

A cross flow model which consists of 100 mm inlet and outlet, 5×0.5 m horizontal channel and 50 mm particle injection opening at 90 degree to the air flow inlet. 102000 quadrilateral cells were used to simulate the model. Simulation result shows that classification of particle occoured by inlet air flow where biggest particle follow straight trajectory because of high inertia where as smaller particles follow longer trajectory. Small range of classification is observed at 5 m/s inlet flow velocity and 5 m/s particle injection velocity showed in Fig. 4.2 which shows that smallest particle follow the inlet air flow because gravitational force is very low that it can not settle or strike at the bottom of channel. Particle of 212 μm follow turbulence vortices created by sudden expansion flow inlet into the channel.

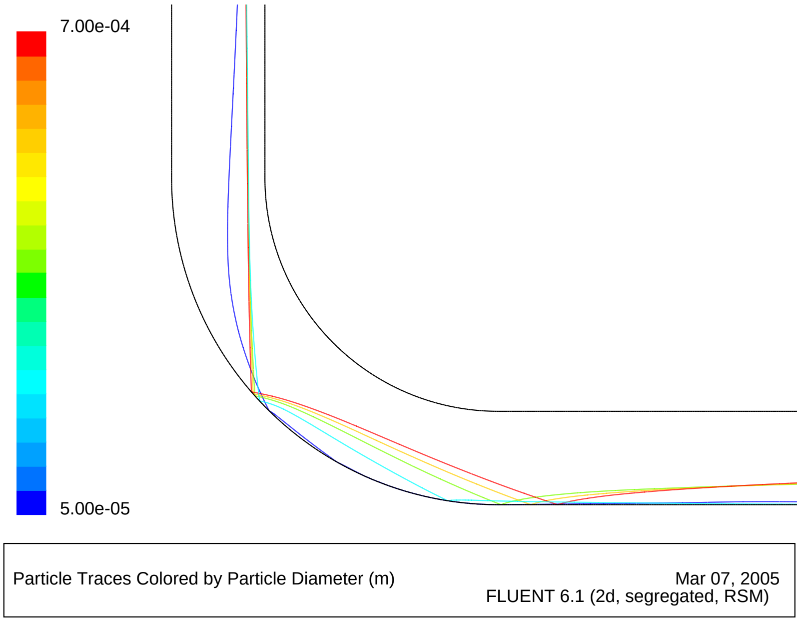

Figure 4.1: Calculated particle trajectories in elbow at inlet air velocity 23 m/s

Modification of inlet of this model (bigger inlet or same inlet with inclined plane) would reduce this effect. Particle wall collision does not have significant effect on classification. This model is not feasible for using at grinding mill outlet because gas and particle are not separated in this case.

Inertia separator

An inertia separator of 100 mm inlet, 80 mm outlet and 350 mm long impactor have been modeled with 24250 computation cells. Simulation results (see Fig. 4.3) show that particles separation is occured after rebouncing off the impactor and all particles above 180 μm settle down at the bottom. Particles below 180 μm size are separated by fluid dynamic effects which follow the flow path overcoming gravitional force.

Channel model

Channel of 0.5 m height, defined length, inlet and outlet 100 mm diameter each and an inclined plane adjacent to inlet was designed to simulate. Simulations have been performed for different inlet velocities with 72767 quadrilateral cells. At the length of 5 m and 1 m/s inlet velocity particle classification was observed (see Fig. 4.4) for wide range of particle sizes where biggest particle has longest trajectory because of relatively higher inertia. The smaller particles have low inertia so that they are easily settled by gravitational force at the entrance of channel.

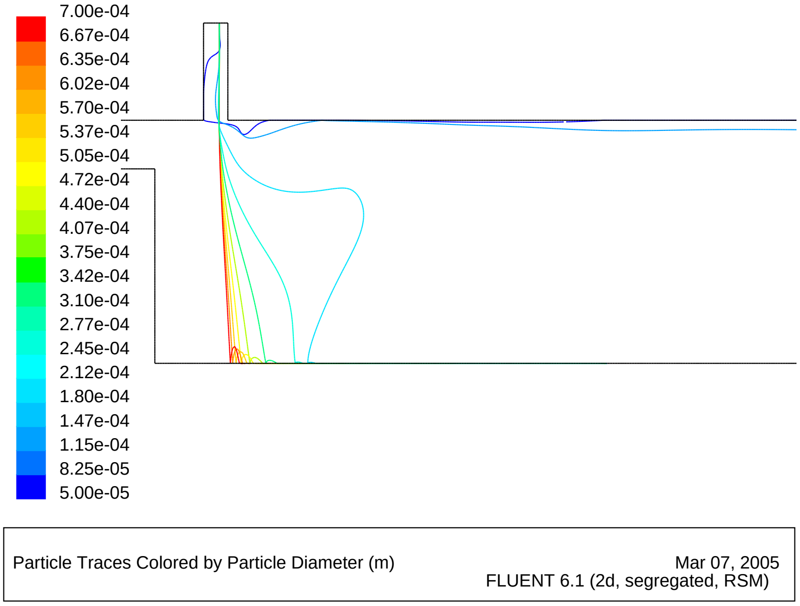

Figure 4.2: Calculated particle trajectories in crossflow model at inlet air velocity 5 m/s

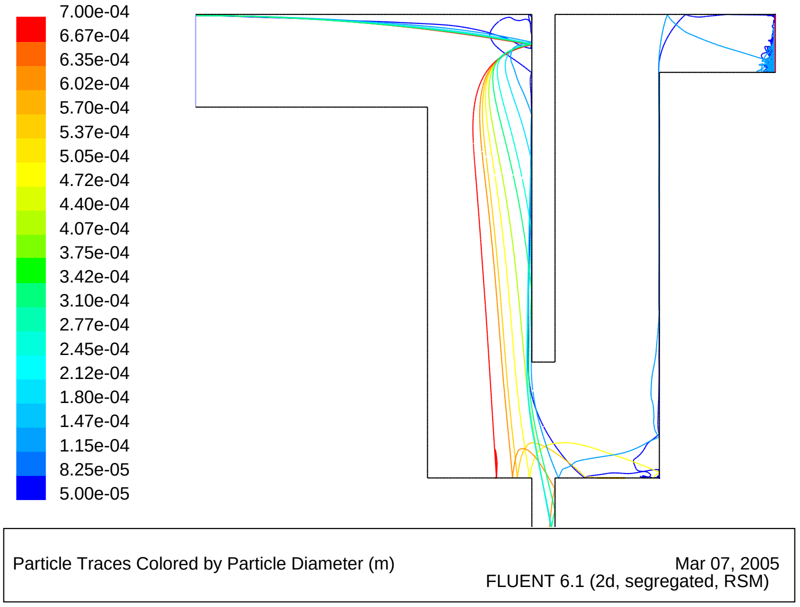

Figure 4.3: Calculated particle trajectories in inertia separator model at inlet air velocity 5 m/s

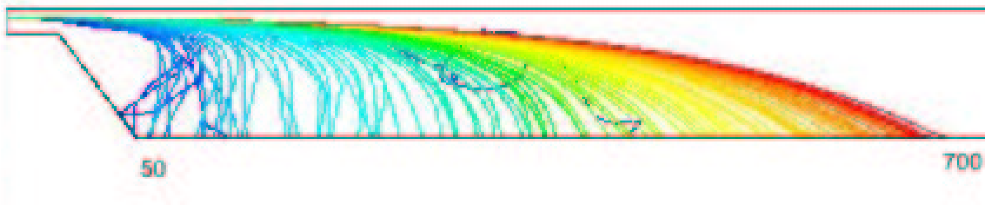

Figure 4.4: Calculated particle trajectories in channel model at inlet air velocity 1 m/s

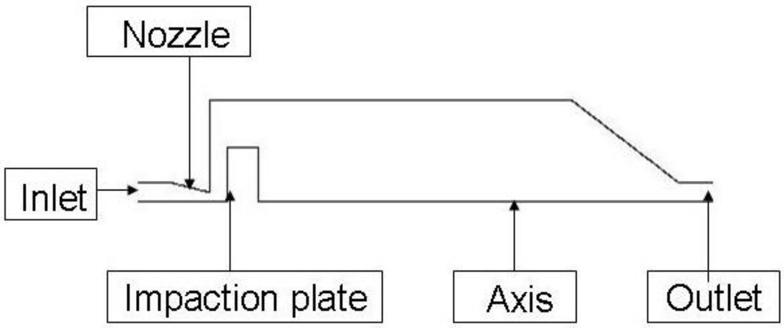

Figure 4.5: Nozzle-Impactor model

4.3 Nozzle-Impactor model

A 100 mm diameter 1 m long pipe, accelerating nozzle of 100 mm diameter inlet 50 mm diameter exit, a 556 mm diameter 1 m long vessel have been connected in series. An impactor of 300 mm diameter has been set at different distance from the 100 mm diameter pipe inside the vessel. Figure 4.5 shows rough sketch of the model and also see figures of chapter 5. By varying inlet velocities and jet impactor distance a number of flow simulations were carried out with 96159 quadrilateral cells and 2D axissymetric domain.

Flow simulation (see Fig. 4.6) shows that there are some turbulent vortices at the corner of the impactor which would have effect on local particle trajectories.

In order to study the single particle behaviour, simulations under single particle injection for 1 to 700 μm were carried out. At 50 mm jet impactor distance simulation results (see Figs. 4.7 and 4.8) show that for an equal tracking time the trajectories of smaller particles were curved (longer path length) while larger particle follow straighter trajectories.

Simulation of this model with surface injection reveals that significant classification occured after particle bouncing off nozzle wall into impactor. Particle wall interaction has significant effect (see Figs. 4.9 and 4.11) on separation of particles in the vicinity of wall while particles away from wall separated by fluid dynamic parameters explained in Sec. 3.2.2. Particle wall collision also separate particle after bouncing off impactor (see Fig. 4.10). Figure 4.10 shows that smallest particle of feed strikes towards center following the narrow flow path within the nozzle while bigger particles do not deviate from its initial path. This means that there is no aerodynamic separation adjacent to center of impactor.

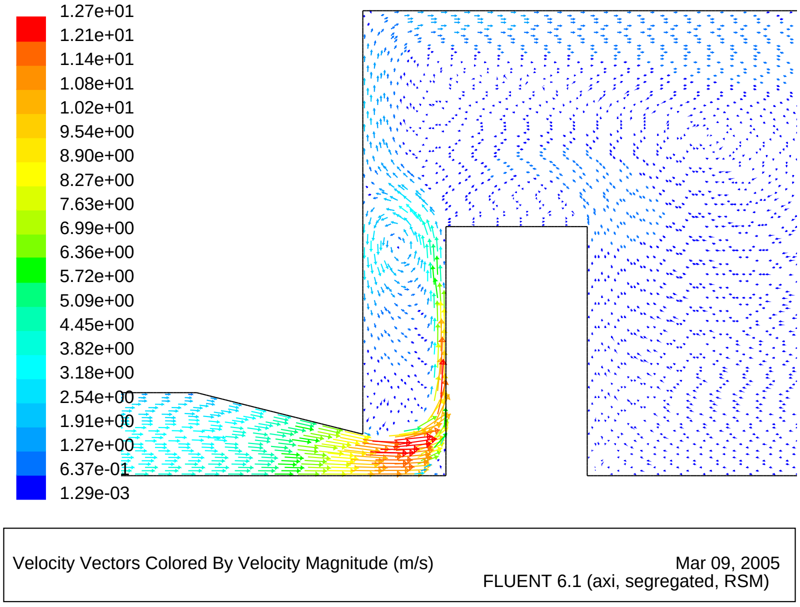

Figure 4.6: Velocity vectors in impactor model at inlet air velocity 3 m/s

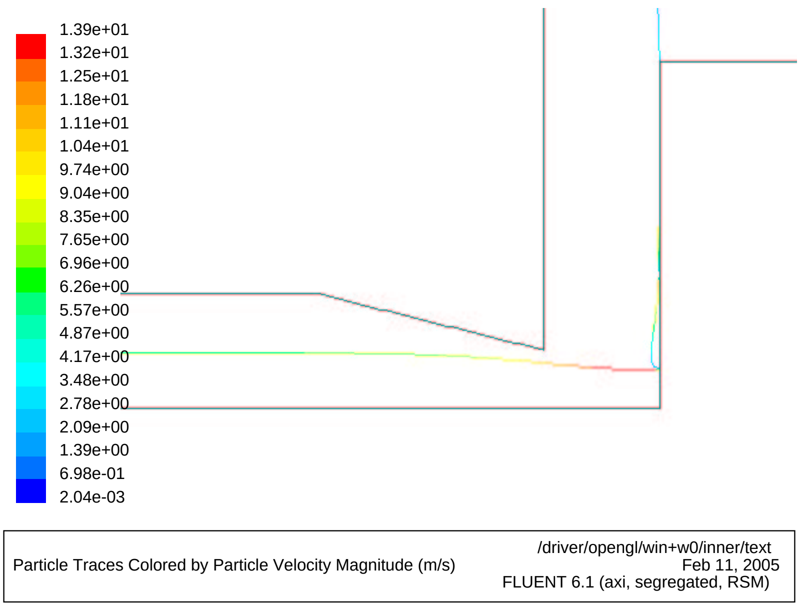

Figure 4.7: Calculated particle trajectories for 700 micron particle in impactor model at inlet air velocity 3 m/s

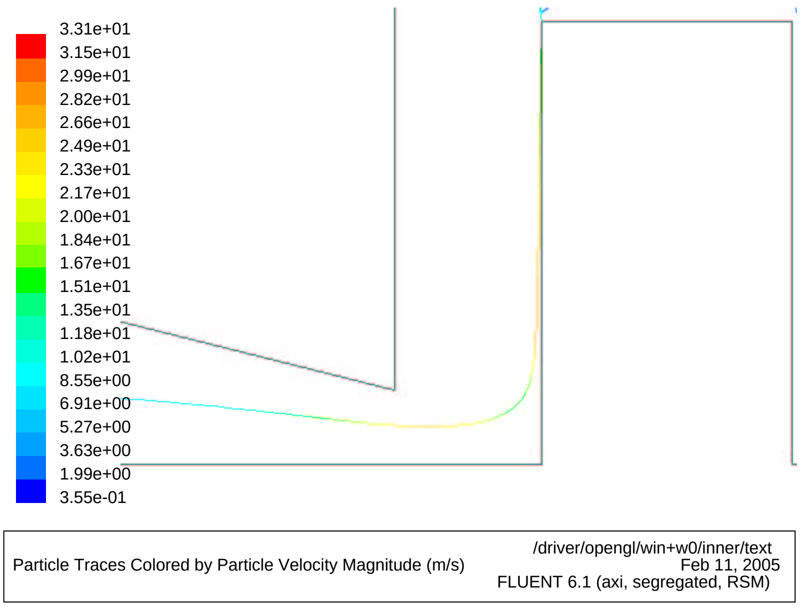

Figure 4.8: Calculated particle trajectories for 1 micron particle in impactor model at inlet air velocity 3 m/s

The smallest particle of feed first strike on 22 mm to 25 mm distant from the center of impactor after rebouncing off nozzle wall and secondly strike on 73 mm to 88 mm from the center of impactor depending on particle stream number. The simulation of the nozzle-impactor shows that most of the bigger particles strike near center of the impactor while smaller particles impact at distant from center of impactor. It is evident that some of the smaller particles impact near center after rebouncing off wall or impactor.

A number of simulations have been carried out by varying coefficient of restitution. Change of coefficient of restitution alter particle trajectories (see Figs. 4.12, 4.11). After particle first bouncing off wall or impactor, where particles will strike again that depends on particle wall interaction parameter (i.e. coefficient of restitution) and particle sizes.

Simulations results reveals that coefficient of restitution has a significant impact on simulation results. It is obvious to know experimental data of coefficient of restitution for reliable modeling. Experimental data of particle inlet velocity would give precision of simulation results. Nozzle-Impactor model among the above simulated models has been chosen to measure particle size which would be applicable to measure particle size by force sensing principle explained in Sec. 3.1.

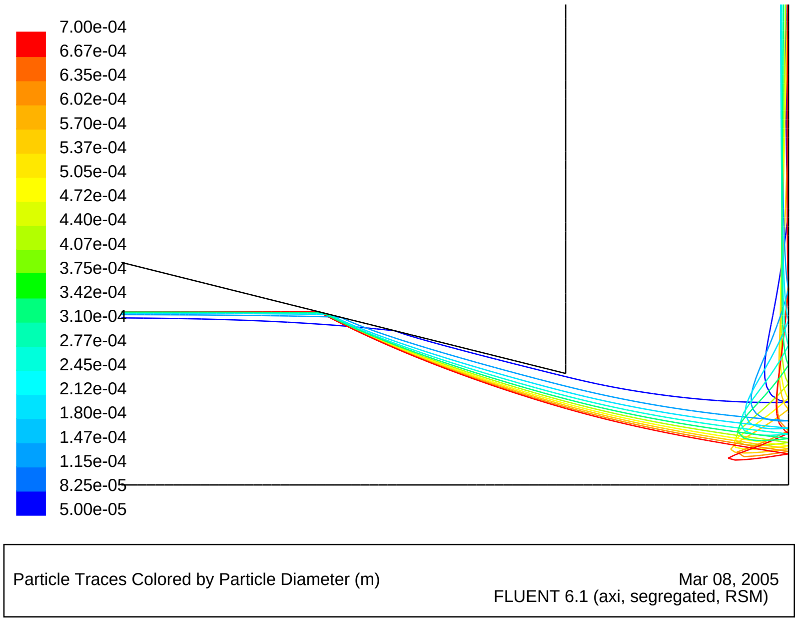

Figure 4.9: Calculated particle trajectories in impactor model at inlet air velocity 3 m/s

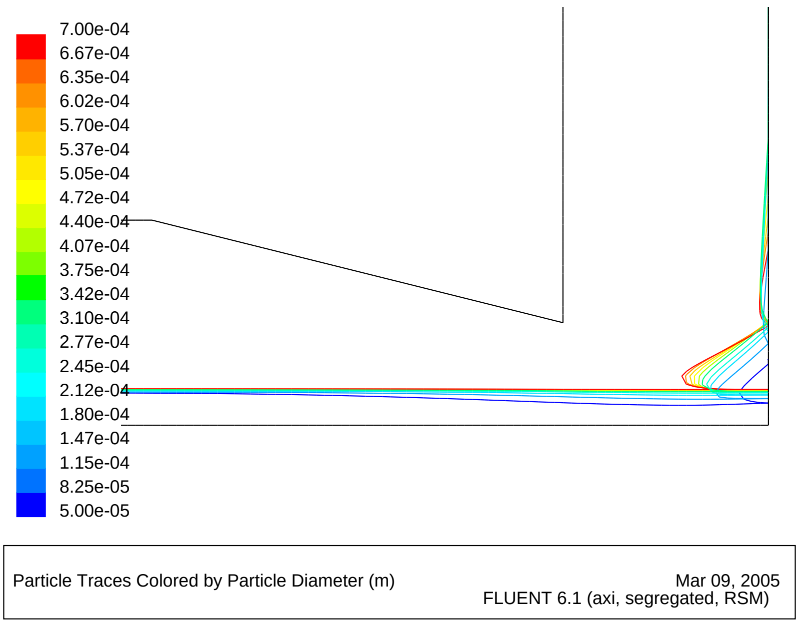

Figure 4.10: Calculated particle trajectories near center in impactor model at inlet air velocity 3 m/s

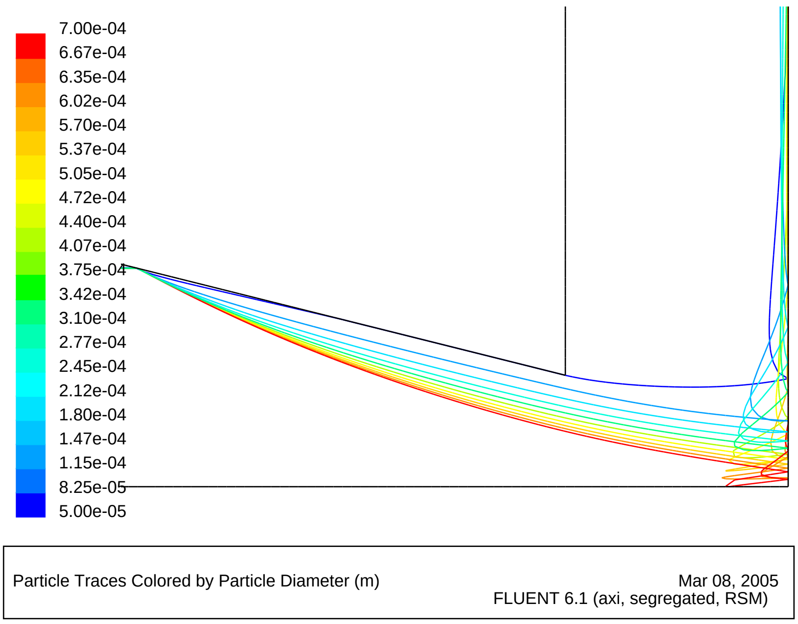

Figure 4.11: Calculated particle trajectories of near wall particles in impactor model at inlet air velocity 3 m/s coefficient of restitution 0.2

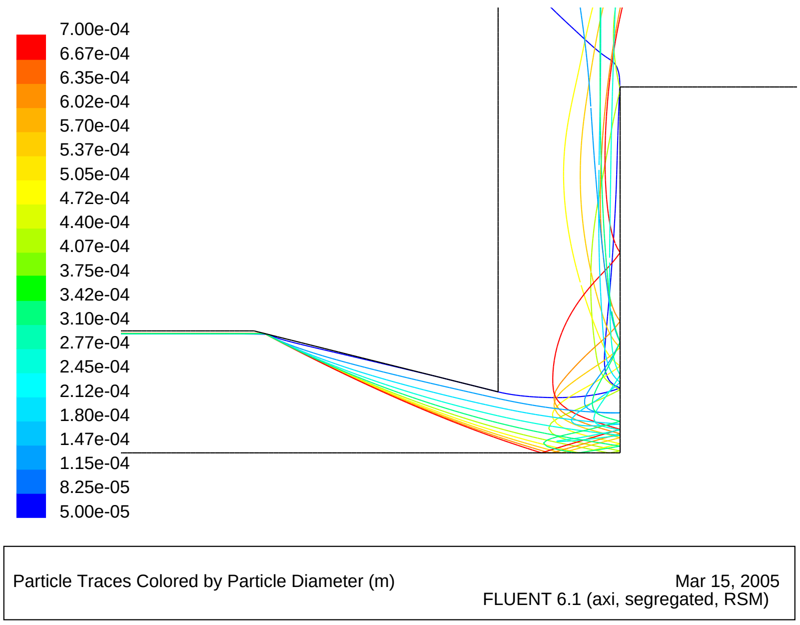

Figure 4.12: Calculated particle trajectories in impactor model at inlet air velocity 3 m/s with coefficient of restitution 0.5

Chapter 5

The Experimental System

This chapter contains the description of experimental set up of the measurement device and calibration of system components.

5.1 Experimental set up of Measurement Device

In order to measure particle size in-line a measurement system was built up. In the real process particles coming out of grinding mill are fed into the system. In this thesis an artificial feeding material stream is maintained by an automatic controlled vibrational feeder. Other than feeder, the measurement system consisted of following system components:

- A 100 mm diameter 1 m long pipe as in inlet
- An accelerating nozzle made of PVC (100 mm diameter inlet, 50 mm diameter exit and 100 mm long 14°)
- A 300 mm diameter impactor plate made of PVC
- A 556 mm diameter 1 m long vessel with removable lid
- A computer controlled blower

The feeder (see Fig.5.1) was set on a wooden basement located 3 m off the ground. The first stage of the system was the 100 mm diameter 1 m long pipe (a in Fig.5.2). In order to get fully developed flow, 1 m long pipe was used. A 100 mm diameter 250 mm long plexi glass pipe (b in Fig.5.2) was connected at the exit of the pipe with a flange (c in Fig.5.2). The plexi glass was used to observe particle-laden flow during particle sampling for size measurement. The plexi glass pipe was connected with a 50 mm long welding end (e in Fig.5.2) which was welded with the lid (f in Fig.5.2). Two plexi glass windows (d in Fig.5.2) were set in lid by screws to observe flow behaviour above the impactor plate. Experiments were performed at first without accelerating nozzle and then with accelerating nozzle. The accelerating nozzle was set with welding end by screws. The impactor was designed and constructed in such a way that its position from pipe exit or nozzle exit could be varied inside the vessel (g in Fig.5.2). This distance is called jet-impactor distance. Detail design of impactor is described in the following section. The vessel exit was connected to the computer controlled blower by a 100 mm diameter pipe.

Figure 5.1: Feeder used for experiment

Figure 5.2: Components of measurement system

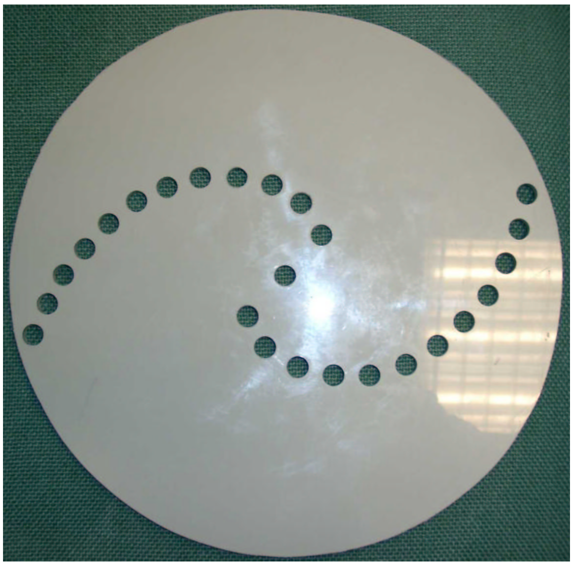

Figure 5.3: Impactor plate design

Description of the impactor

The 300 mm diameter impactor top plate consisted of 25 circular openings of 10 mm diameter each where one of them located at the center of the plate. Each half circle consisted of 12 openings. Each half circle was divided into 12 zones based on distance from the center of impactor (radial distance) and angular positions as shown Fig.5.3. The openings were spirally positioned in order to maintain maximal distance of individual opening from the center and to get maximum number of sampling positions. In order to investigate the symmetry of collected particle size of both sides, both half was designged in an aligned fashion. In this design each opening was assumed to be representative of defined radial and angular position. The impactor plate was made of PVC to minimize particle bounce and flow disturbance of rough surfaces of impactor plate. The impactor plate (p in Fig.5.4) was bolted to strong wooden basement (r in Fig.5.4) of same diameter as impactor plate by screws. The wooden basement was fixed with three steel made beams (s in Fig.5.4) aligned by welding. The angle between each beam was 120 degree. The center of the wooden basement was kept at the connecting portion of beams. The outer section of each beam was used to connect with three screw stands (t in Fig.5.4) where each of them was 1 m long. These stands were used to hang the impactor from the lid of the vessel to maintain jet impactor distance (d in Fig.5.4). In order to insert the screw stand into the lid three holes were made in lid maintaining similar position of screw stand of beams and screw was used to fix the stand with lid. In between impactor plate and basement another circular plate of same diameter as impactor plate was used to hold cylindrical Particle Sampling Bins (PSB) made of plastic as shown in Fig.5.5. Each PSB has 13 mm diameter and 48 mm height and this plate was designed as the similar way of impactor plate. Every PSB has its own identification number. PSB at center is C and adjacent to center in one half circle the first PSB is called C1-1 and the next are C2-1,C3-1 and so on until C12-1 while for the another half circle, the first one is C1-2 and the others are C2-2 to C12-2 successively.

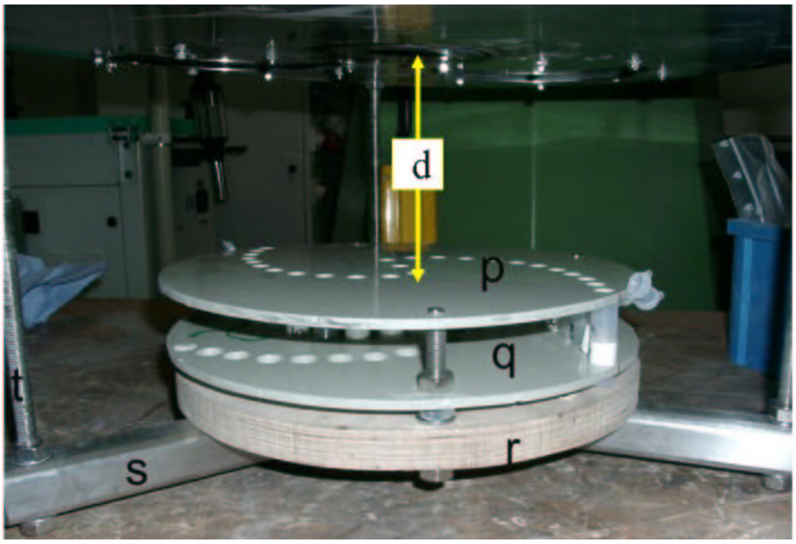

Figure 5.4: Impactor component

Figure 5.5: Impactor component

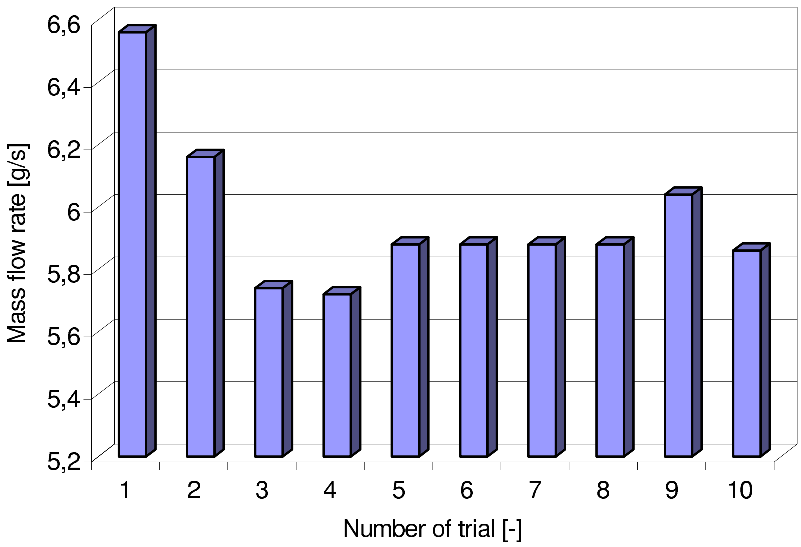

Figure 5.6: Unsteady massflow rate of feeder at control range 8

5.2 Feeder calibration

An automatic controlled vibrational feeder was used to get definite mass flow rate control range is defined from 1 to 10. It is designed by manufacturer in such a way that feeding range increase with increasing number of range. For each control range a constant feed rate should be maintained by feeder. In fact, it slightly varies with number of trials at a fixed control range. Feed material contains different sizes and shape of particles. Interaction of those particles and conveying line of feeder results unsteady type of particulate flow. In every 5 seconds solid mass flow has been measured for control range 7 and 8. These results show that mass flow rate is not constant for each trial. It slightly varies for each trial. Experimental result of control range 8 is in Fig.5.6. The arithmetical average of mass flow rate of control range 8 is 6 g/s or 21.6 kg/h.

5.3 Air velocity measurement at the system inlet pipe

A computer controlled blower was used to establilish air flow as well as particle flow into the system. The blower can work at wide range of speed which is defined as rotor number of revolution per minute (rpm). The blower creates vacuum which draws air towards the blower. A Prandtl sensor was used to measure air velocity at the system inlet pipe for different rpm. The Prandtl sensor measures pressure at the system inlet pipe and convert it into velocity by the following equation [6]:

$$v = \sqrt{\frac{p}{\frac{\rho}{2} + \frac{p}{2}c^2}} \tag{5.1}$$

$$\rho = 1.292kg/m^3 + 273/(273 + T) \tag{5.2}$$

Where ρ= air density, p= air pressure in Pa, T= air temperature in celcius and c= velocity of sound in air in m/s The results are shown in Fig.5.7. The results show that air velocity

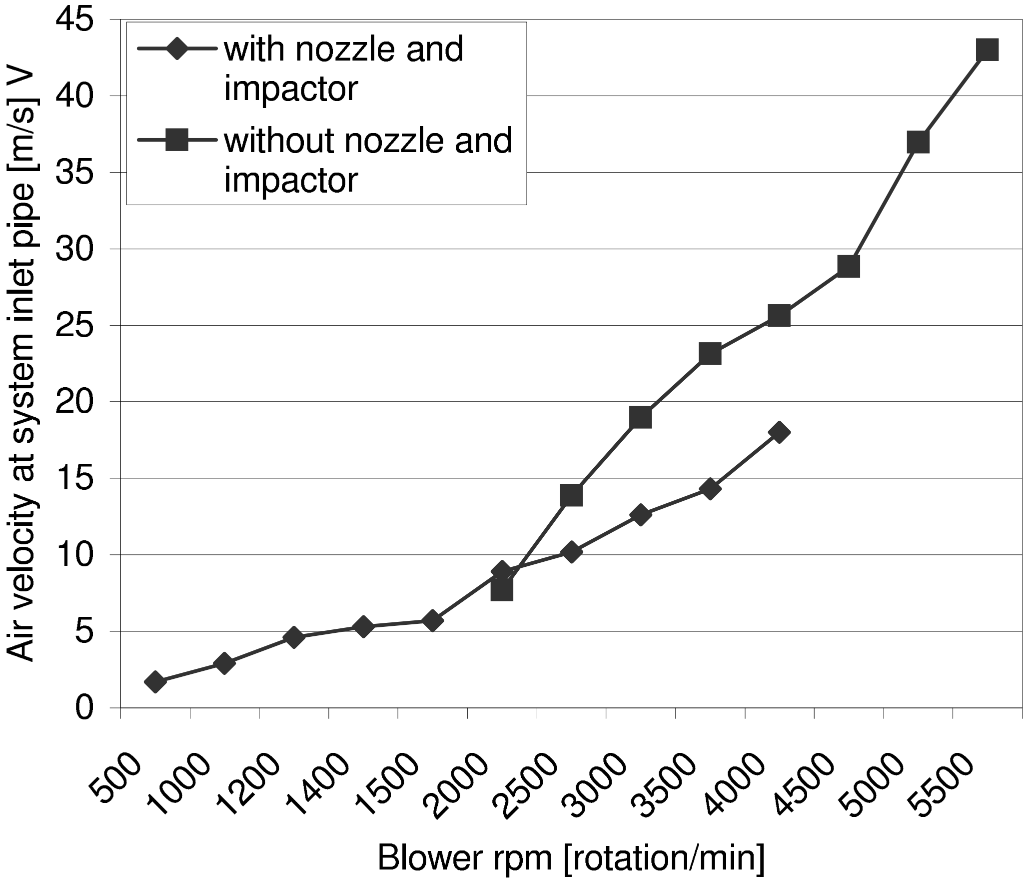

Figure 5.7: Air velocity at system inlet pipe vs blower rotor rpm

at the system inlet is higher in case of without any hindrance into the system. When nozzle and impactor present into the system, significant pressure drop occur which reduces the air velocity at the system inlet.

Chapter 6

In-line Particle Size Measurement by New System

This chapter contain description of particle sampling process and particle sizing method used in this thesis.

6.1 Particle sampling

For each measurement the blower was started with a specific rpm and thermoplastic material (TPU) particles were injected by the feeder at the average solid feedrate of 21.6 kg/h. Some amount of particles flown into the system is settled in PSB and the rest amount of particle flows towards the blower which is trapped into a filter set just before the blower. After 5 minutes of feeding the feeder and blower were shut down and the impactor was taken out from the vessel by removing the lid. The PSB were collected from the impactor and stored for particle sizing in laboratory by laser diffraction instrument.

6.2 Off-line particle size measurement

Particles collected by PSB have been measured off-line by laser diffraction instrument called MasterSizer manufactured by Malvern.

MasterSizer has four major components such as transmitter (L), sampling volume (S), detector (D) and sample suspending tool (H). Fig.6.1 shows the MasterSizer used in this thesis. Particles are suspended in suspending medium and the suspension is pumped to the sampling volume of the instrument. A low power Helium-Neon laser ($\lambda = 632.8nm$) forms a collimated and monochromatic beam. When a collective of particles is introduced into the laser beam in the sampling volume, a Fourier lens projects the far field diffraction pattern of the scattered light at the focal plane. This optical configuration has the characteristic that a moving particle at the position in the laser beam always causes a stationary light intensity pattern that is centered on the optical axis. The diffraction pattern is collected by a multi-element detector along the radial direction of the focal plane. By means of scatter model and numerical optimization technique PSD can be back calculated. Different scatter models and numerical treatment techniques are avialable which is described in detail in [7].

Figure 6.1: MasterSizer used for particle sizing

The measurement results depend on dispersibilty of particle in the dispersion medium. For this thesis water was used dispersion medium along with surfactant called Na Dodecylbenzen 0.5% Sulphonate. Mechanical energy was supplied to the suspension by using stirrer to get well dispersed suspension. 2000 rpm was used as stirrer speed. Fraunhofer model as scatter model was used because this model does not need material or medium optical properties. The scattering is mainly caused by diffraction of light around the particle. This makes the Fraunhofer theory only valid for a limited range of scattering angle and particle size parameter α. $\alpha = \frac{\pi x}{\lambda}$ where x is the particle size and λ is the wavelength of incident light. Particles are assumed to be spherical during calculation of PSD.

6.3 Sources of error of the laser diffraction instrument

Gommeren [7] experimentally showed that laser diffraction instrument undersize or oversize the measured particles if irregularly shaped particles are present in the sampling volume of instrument. The other sources of error could be as follows:

- Theoretical errors such as incorrect light scattering models used by instrument
- Differences in the nature of product such as non-homogeneity of particles
- Excess use of surfactant for dispersing in water.

All of the above mentioned factors make the prescription of a standard process for measurement very difficult but not impossible.

Chapter 7

Results and Discussion

The system was evaluated for its ability to deliver representative samples while the impactor and its PSB were evaluated in terms of collected particles median size (x_{50}). The sampling duration of all the runs were kept constant for 5 minutes.

7.1 Experimental results without accelerating nozzle

First experiments were performed without accelerating nozzle at the exit of system inlet pipe by varying air velocity at the system inlet and jet-impactor distance. TPU particles of 271 μm median size (see Fig.7.1) were fed into the system and were collected into the PSB located in the impactor. All results are expressed in terms of median particle size.

At 23 m/s air velocity at system inlet pipe and 100 mm jet-impactor distance PSB C collects 267 μm median particle and PSB C5-1 collects 204 μm median particle and in case of PSB C6-1 to C12-1 collected particle size increase with increasing PSB number i.e. radial distance from the center of impactor (see Fig.7.2). All other results are also expressed in terms of median particle size. At 23 m/s air velocity at system inlet pipe and 50 mm jet-impactor distance PSB C collects 260 μm particle while PSB C3-1 collects 190 μm particle and starting from PSB C4-1 particle size increase with the increasing radial distance (see Fig.7.3). These two experimental results show that particle classification range increase with decreasing jet-impactor distance. Minimizing jet-impactor distance compels a particular air stream to move at the radial direction of impactor plate and

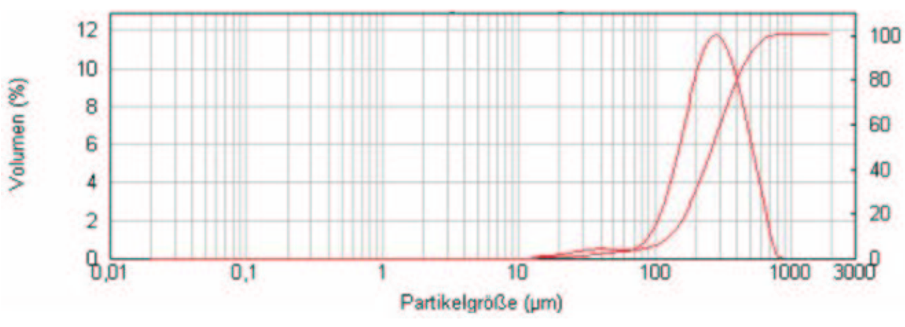

Figure 7.1: Feed particle (TPU) size distribution

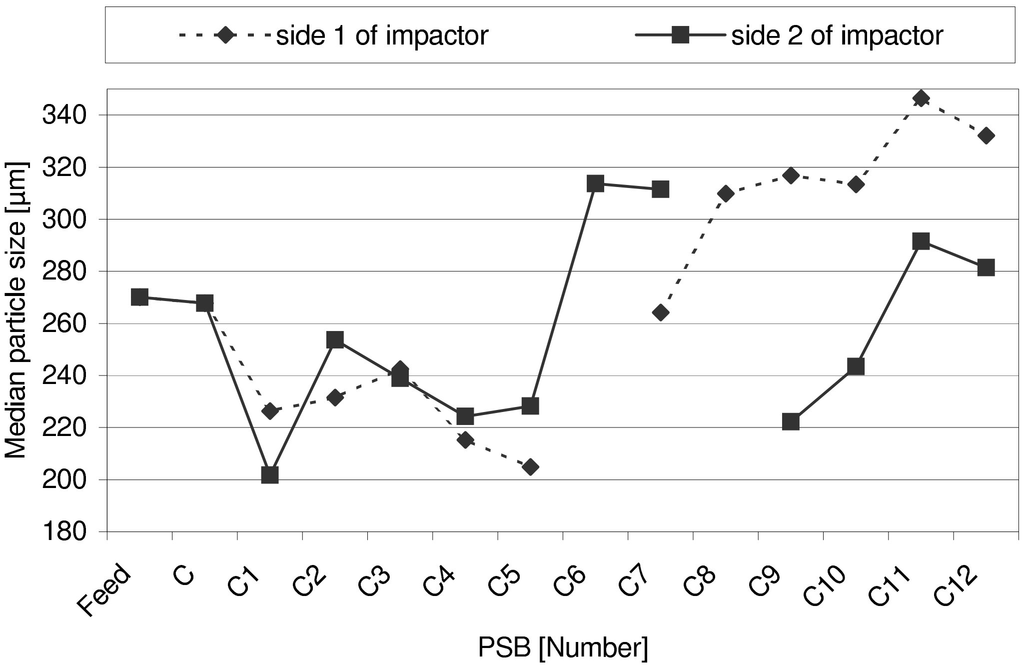

Figure 7.2: In-line PSD at 23 m/s and 100 mm jet-impactor distance

smaller particle follow this air stream. Due to this reason in the second case PSB C3-1 collects smaller particle than that of first case.

By fixing jet-impactor distance at 50 mm and increasing air velocity at system inlet a wide range of particle classification was observed as shown (see Fig.7.4) where PSB C collects 224 μm particle and PSB C5-1 collects 57 μm particle. Increasing air velocity increases drag forces acting on particle depending on particle sizes which helps particle to be classified.

From the above experimental results, it has been observed that collected particle size decreases except some deviations with increasing radial distance from the center of impactor until certain distance depending on air velocity at system inlet. After certain radial distance of impactor particle size again increase. This increasing particle size with increasing radial distance may be due to local turbulent vortices at the outer section of the impactor. Particle follow turbulence according to their individual Stokes number and settle in the local bins according to gravitational force acting on them. Some of the bins collect bigger sizes particle than their previous bin which may be due to irregular shaped particle present in sample during laser diffraction measurement (see Sec. 6.3) or local flow disturbance because of measurement system construction. This can also be for the individual particles due to stochastic disturbances or bouncing of particles off impactor plate. It has been also found that both sides of the impactor do not show symmetry of particle collection. In Figs. 7.2-7.4 two different lines show collected particle size of two sides of the impactor. Both side was not geometrically similar because of presence of lid window or screws in side two (see Fig.7.5) in the second side of impactor which would disturb the local flow path. Other construction problem was also encountered in the measurement system such as the lid was not horizontal as a result the inlet pipe of the system was not

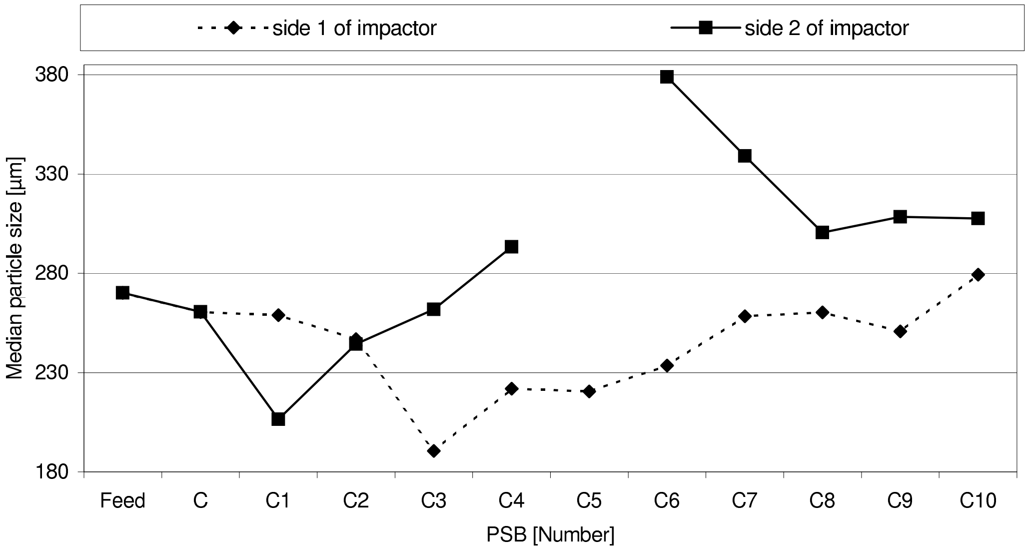

Figure 7.3: In-line particle median size at 23 m/s at inlet and 50 mm jet-impactor distance

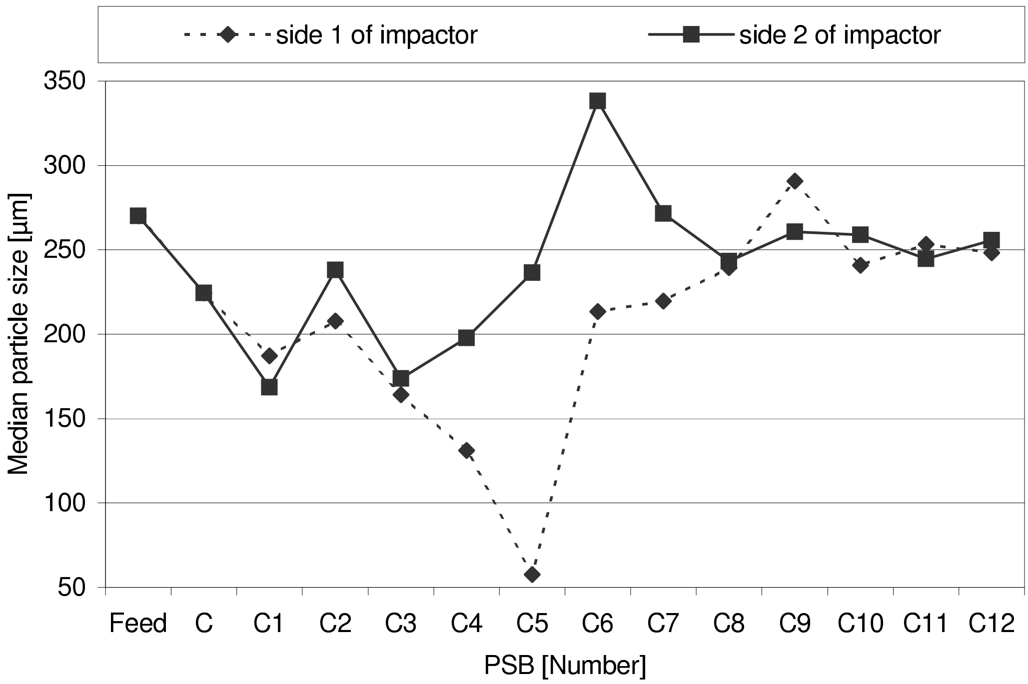

Figure 7.4: In-line PSD at 43 m/s

Figure 7.5: Bottom of the lid in the measurement system

Case	Flow at inlet [m/s]	Feed [μm]	C [μm]	C8 [μm]
1	14.2	215	209	142
2	11.6	215	215	127
3	5.7	215	215	65
4	2.9	215	204	67
5	1.7	216	216	87

Table 7.1: Summary of experimental results

vertical. Some bins were empty after collection from the vessel. This may occured beause of particle dropping from those bins during sample collection.

7.2 Experimental results of Nozzle-Impactor model

Observation of the results in Sec. 7.1 reveals that smaller size particles obtain larger radial velocity component (tangent to the impactor plate) which increase with increasing air velocity at the system inlet as well as above the impactor plate. This idea lead to construction of the accelerating nozzle at the exit of system inlet pipe in order to get wider range of particle size distribution along the radial position of the impactor. Experiment was carried out with Nozzle-Impactor model which is able to clssify wider range of particle size depending on air velocity at system inlet pipe and 50 mm jet-impactor distance. The results were presented in Fig. 7.6. Experiments were performed for five different inlet conditions see Tab. 7.1 and 50 mm jet-impactor distance

The nozzle accelerates the flow and every case the velocity of the flow at the exit of the nozzle is about 4 times higher than that of at inlet (See Fig. 4.6). This incremental velocity is the major driving force for the particle classification as shown from the experiments. For each case feed particles were classified into 9 bins and Tab. 7.1 shows summary of the results.

For all cases, particle size decreases until PSB C8-1 with increasing radial distance of impactor except some deviations. The reason of deviations explained in previous section. Particle size increases starting from PSB C9-1 due to turbulent vortices at the outer section of impactor plate which is explained in previous section. The second side of the impactor

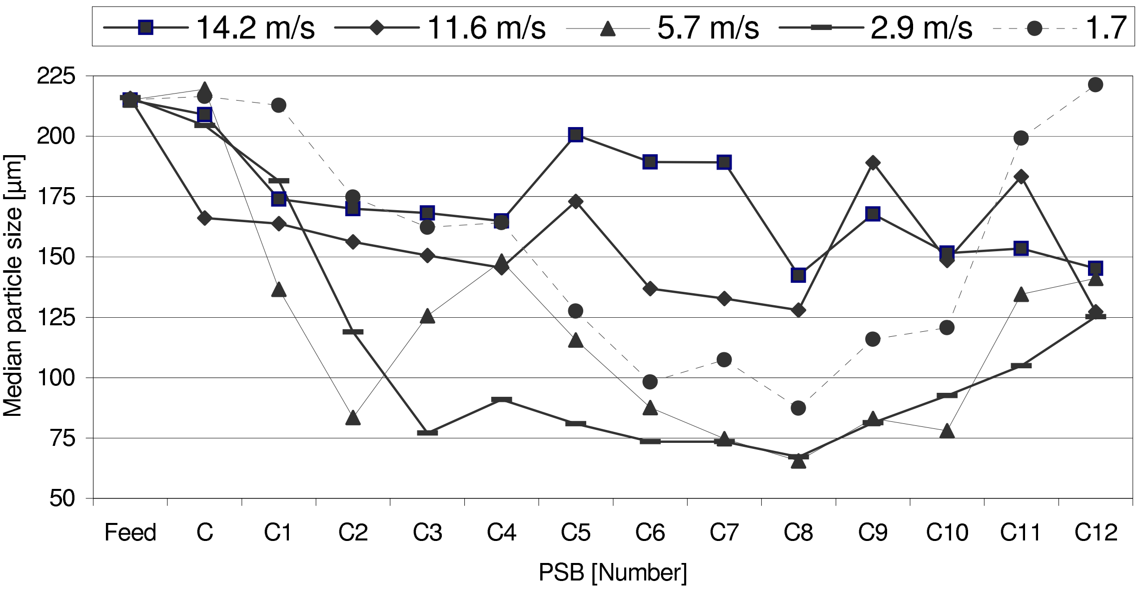

Figure 7.6: Effect of air velocity at system inlet on in-line PSD

does not show the symmetry of collected particles due to geometrical dissimilarity as described in previous section.

Fig.7.7 shows that in case of Case 3 and 4, impactor collects wider range of classified particle where range is calculated from the difference between collected biggest median size and smallest median size of particles by bins. Among these two cases well distributed particle classification without fluctuation was observed in case of Case 4. In case of Case 1, the median size of particles collected by PSB C8-1 is 142 μm. This shows that at higher air velocity smaller particle obtain relatively higher radial velocity component than smaller particle at lower air velocity which make it travel longer radial distance along the impactor. At higher velocity fluctuations increase may be due to stochastic disturbance or unsteady solid feed rate of feeder (see Sec. 5.6). So from the results it reveals that major design parameter of the device is velocity at the system inlet and for the prescribed TPU of defined PSD, 2.9 m/s air velocity at system inlet sharp classification without fluctuation was observed. Figures 7.8 and 7.9 shows density distribution and cumulative size distribution of collected particles for Case 4. Results show that PSD shifted to lower value as the radial distance of impactor plate increase. Bigger particle of feed present almost for PSD of all PSB which decrease classification efficiency of individual PSB.

7.3 Validation of CFD results

CFD simulation results of the Nozzle-Impactor model show that smaller size particles strike distant from center of impactor while bigger particles strike near center. Experimental investigation shows similar results. For exact validation of the simulated results 50 micron particle of the feed in case of Case 4 has been considered. Experimental results and CFD calculations both show that the smallest size particles are present in differnt bins. Experimental result reveals that significant volume percent of 50 micron particle found

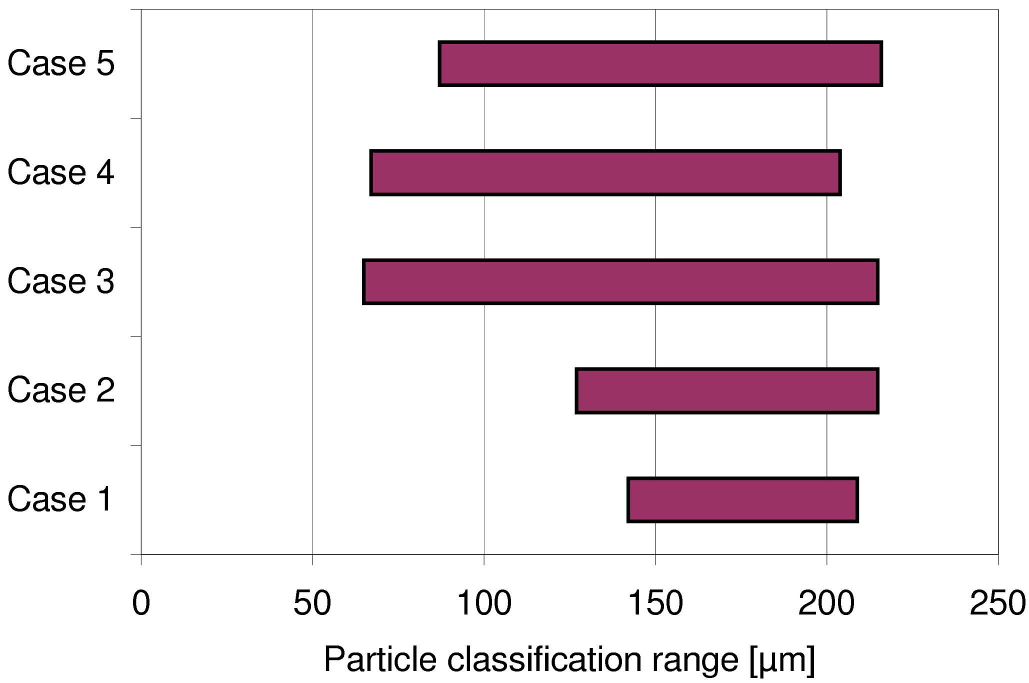

Figure 7.7: Range of classification at different inlet condition of Nozzle-Impactor model

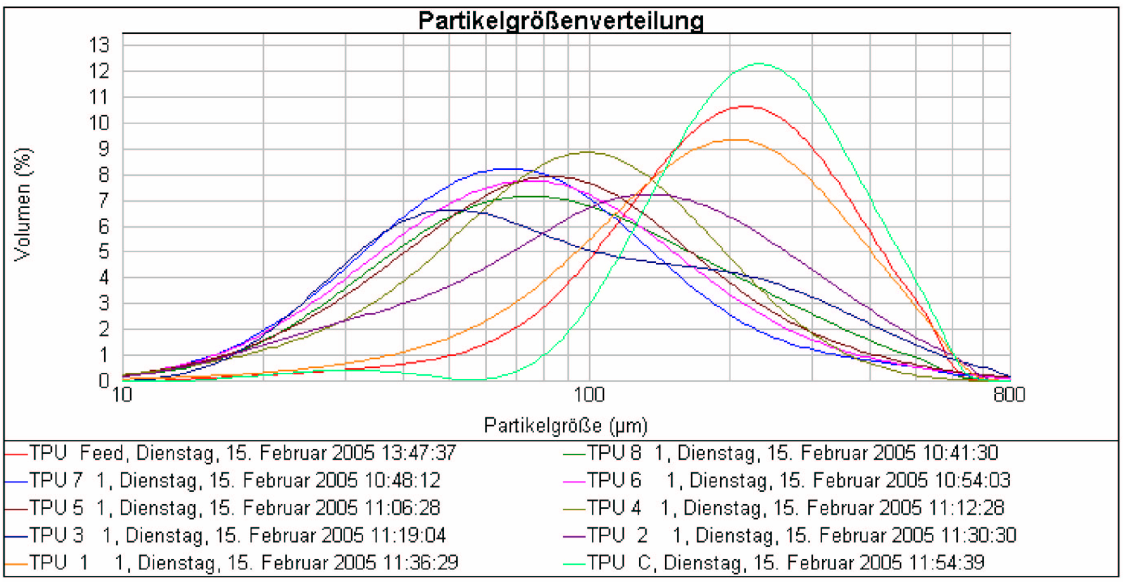

Figure 7.8: PSD (density distribution) of different PSB at Case 4

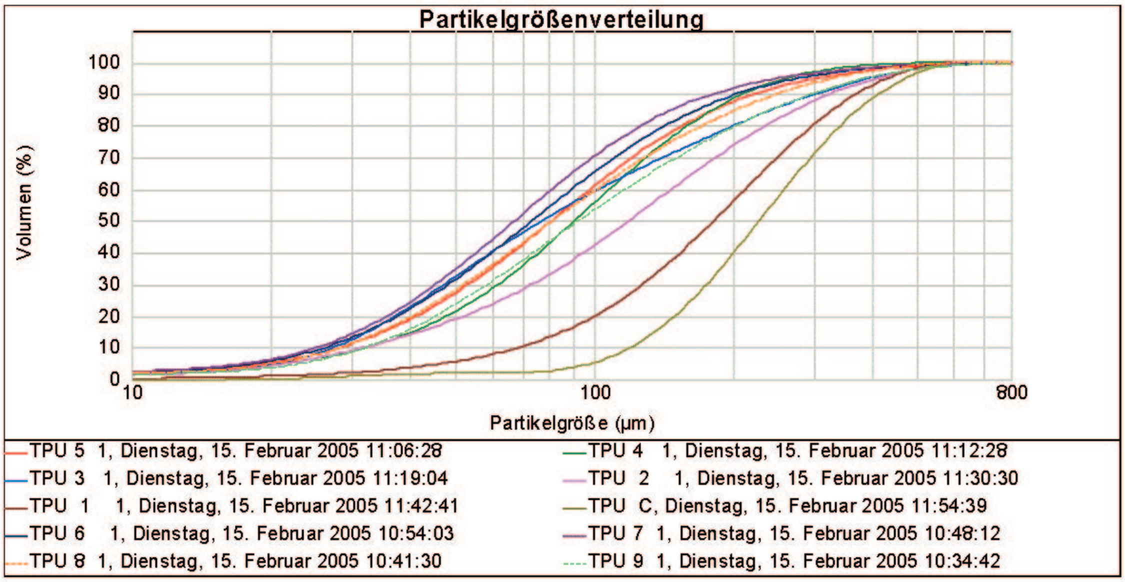

Figure 7.9: PSD (cumulative size distribution) of different PSB at Case 4

in C2-1 (28 mm from center) to C8-1 (95 mm distant from the center of impactor plate) as shown in Fig. 7.10 while CFD calculations show that the same size particle hits 22 to 88 mm distance from the center depending on number of particle stream (see Sec. 4.3). Fig. 7.11 shows the validated results. Simulated results are reasonable with respect to the experimental results.

7.4 Conclusion

A new in-line particle size measurement device has been designed which can classify wide range of particle size by using aerodynamic particle classification principle. This robust method is capable to measure representative particle size of grinding mill outlet. The designed in-line particle size measurement device was successful to classify particle size based on median size of particle (x_{50}). This implies some smaller and bigger particle other than median size always present in the classified particle. A careful construction of the in-line measurement device and further modification of the impactor plate design may improve particle classification efficiency of PSB. The future work involves automation of particle size measurement by sensing impact force of different size class particle. Piezo force sensor can measure impact force delivering output as voltage signal as described in Sec. 3.1. Calculation shows that impact force of 50 μm 1 million particles is about 6 mN ($F = m_p a_p$) while commercial available piezo force sensor [16] can sense until 1 mN. The sensor should mount in place of PSB of the impactor which requires 9 sensors in order to measure 9 classified particle impact. Each sensor would show different voltage signal during impact measurement. Selection of appropriate sensor and sensor array output signal processing would be future research interest.

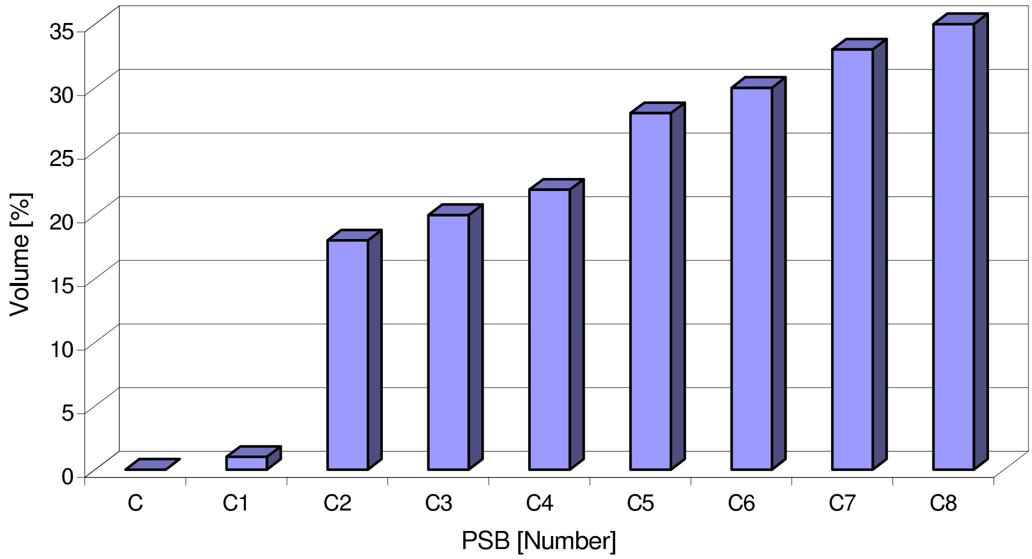

Figure 7.10: Experimental results : relative volume percent of 50 micron particle in PSB

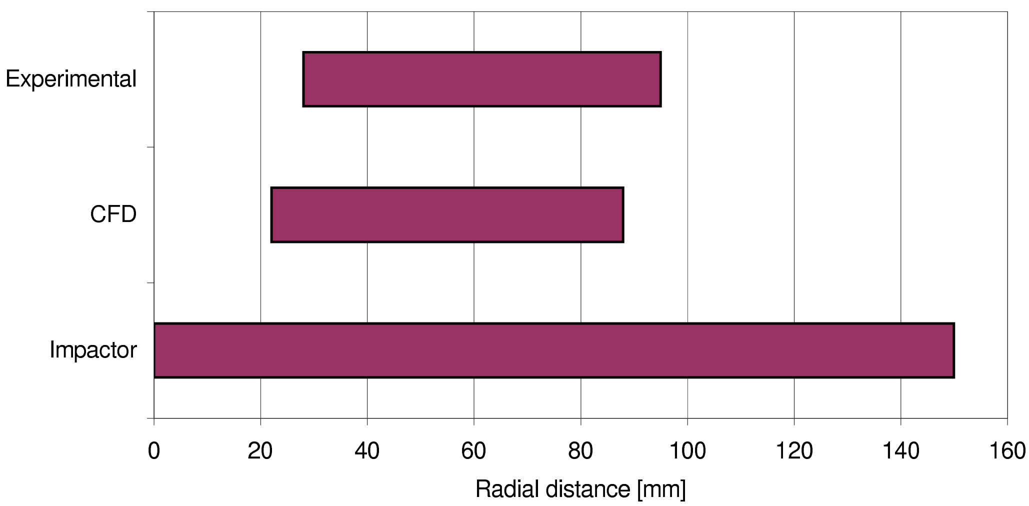

Figure 7.11: Striking position of Plate by 50 micron particle

Summary

Particle size distribution determines greatly the behavior of the material in succeeding unit operations such as chemical reactions, combustion or coating. In-process or in-line particle analysis is key to optimising particulate process and improving product quality. No proven devices are currently available for inline monitoring of particle size distribution (PSD). Available modern measuring methods based on laser diffraction or the coupling of digital camera technology and software-supported image analysis represent so far no optimal solution. Representative particle sampling is not is not possible by conventional methods. Furthermore the investment costs are high. In this thesis, a new inline measurement method has been developed by which representative sampling is possible and the investment cost would be less.

New measurement method based on particle size classification by air flow and force sencing of different sized class particle by piezo sensor.

In order to investigate effect of physical phenomena influencing particle classification detail study of air-particle flow at the designed systems. CFD simulation of different models have been carried out to calculate particle trajectories in the models. Among all simulated models one model called Nozzle-Impactor model was chosen considering ability of classification and particles impact.

Chosen model was built for experimental investigation of particle size in line. Experimental results are presented in this thesis. The newly designed in-line measurement device is capable to classify wide range of particle size by which representative sampling of material coming out from the particulate process is possible. The future work involves automation of the classified particle size measurement by using sensor.

Zusammenfassung

Die Partikelgrößenverteilung bestimmt das Materialverhalten in vielen nachfolgenden Unit-Operations wie chemischen Reaktionen, Verbrennungen und Beschichtung. In-process oder in-line Partikelmesstechnik ist der Schlüssel bei der Optimierung von Partikelprozessen und zur Verbesserung der Produktqualität. Heutzutage sind keine Messverfahren zum zuverlässigen Inline-Messen von Partikelgrößen bekannt. Moderne Messmethoden auf der Basis von Laserbeugung oder digitaler Bildauswertung stellen keine optimale Lösung dar. Die repräsentative Probennahme ist bei den konventionellen Methoden nicht immer gewährleistet. Darüberhinaus sind die Investitionskosten sehr hoch. In dieser Arbeit wurden eine neue Inline-Messtechnik entwickelt, die die repräsentative Probennahme ermöglicht und zudem einfach und kostengünstig ist.

Die neue Messmethode basiert auf der der Auftrennung der Partikelkollektive durch den Luftstrom und der Kraftmessung beim Aufprall der verschiedenen Größenklassen auf der Prallplatte durch Piezo Sensoren.

Zur Untersuchung der physikalischen Phänomene wurden CFD Rechnungen partikelbeladener Strömungen durchgeführt. Aus verschiedenen Konfigurationen wurde schließlich ein Modell (Nozzle-Impactor-Modell) ausgewählt.

Dieses Modell wurde experimentell untersucht und die Ergebnisse sind in dieser Arbeit beschrieben. Es wurde gezeigt, dass die neue Konfiguration einen großen Bereich von Partikelgrößen aufteilen kann.

Im weiteren ist eine Automatisierung der Größenmessung durch Einsatz von geeigneten Sensoren nötig.

Appendix A

Notations

C_D	drag coefficient $[-]$.
$C_D, stokes$	Stokes drag coefficient $[-]$.
D_p	particle diameter $[m]$.
$\vec{F}_g$	gravity force $[N]$.
$\vec{F}_i$	force acting on a particle$[N]$.
$\vec{g}$	gravity vector$[m/s^2]$.
I_p	moment of inertia $[N]$.
Kn	Knudsen number$[-]$.
m_p	mass of particle $[kg]$.
Re_p	particle Reynolds number $[N]$.
$\vec{T}_g$	gravity force $[N]$.
η	mass loading $[-]$.
m_F	mass of fluid $[kg]$.
μ_F	viscosity of fluid$[N-m/s]$.
$\vec{u}_p$	particle velocity $[N]$.
$\vec{u}_F$	fluid velocity $[N]$.
$\vec{\omega}_p$	angular velocity of particle $[N]$.
$\vec{x}_p$	position vector of particle$[N]$.
ρp	particle density $[kg/m^3]$.
ρF	fluid density $[kg/m^3]$.
τ	shear stress $[N/m^2]$.
τ_p	particle response time $[s]$.
τ_F	characteristic time scale of flow$[s]$.
λ_p	particle response distance $[m]$.
ω_t	terminal velocity of particle $[m/s]$.
St	Stokes number $[-]$.
τ_c	time between collisions $[kg/m^3]$.
f_c	collision frequency of particle $[kg/m^3]$.
a_p	acceleration of particle $[m/s^2]$.

Terms

PSD	Particle Size Distribution.
CFD	Computational Fluid Dynamics.
DNS	Direct Numerical Simulations.
PSB	Particle Sampling Bins.
TPU	Thermoplastic Urathene
PVC	Poly Vinyl Chloride.

Bibliography

[1] Coulson and Richardson. *Chemical Engineering Volume 2*. Wiley and Sons, USA.

[2] C. T. Crowe, M. Sommerfeld, and Y. Tsuji. *Fundamentals of Gas-Particle and Gas-Droplet Flows*. CRC Press, Boca Raton,USA, 1998.

[3] S. Elgobashi. On predicting particle laden turbulent flows. In M. Sommerfeld, editor, *Proc.7th Workshop on Two Phase Flow Predictions*, 1994.

[4] S. Elgobashi and G. C. Truesdell. Direct simulation of particle dispersion in a decaying isotropic turbulence. *J.Fluid Mechanics*, 242:655–700, 1992.

[5] D. Eskin and H. Kalman. Engineering model of friction of gas-solids flow in a jet mill nozzle. *Chemical Engineering Technology*, 25(1), 2002.

[6] Ahlborn Mess-Regeltechnik GmbH. *Prandtl sensor User Guide*.

[7] E. Gommeren. *Study of closed circuit jet mill plant using on-line particle size measurement*. PhD thesis, Delft University of Technology, 1997.

[8] A. Haider and O. Levenspiel. Drag coefficient and terminal velocity of spherical and nonspherical particles. *Powder Technology*, 58:63–70, 1989.

[9] C. Heffels, R. Polke, M.Raedle, B. Sachweh, M. Schaefer, and N. Scholz. Control of particulate processes by optical measurement techniques. *Part. Part. Syst. Charact.*, 15:211–218, 1998.

[10] H. H. Hu. Direct simulation of flows of solid-liquid mixture. *Int. J. Multiphase Flow*, 22:335–352, 1996.

[11] N. Huber and M. Sommerfeld. Modelling and numerical calculation of dilute-phase pneumatic conveying in pipe systems. *Powder Technology*, 99:90–101, 1998.

[12] N. Huber and M. Sommerfeld. Experimental analysis and modelling of particle-wall collisions. *Int.J.Multiphase Flow*, 25:1457–1489, 1999.

[13] Fluent Incorporated. *Fluent User Guide*. 2003.

[14] G. Kohnen, M. Rger, and M. Sommerfeld. Convergence behaviour for numerical calculations by euler/langrange method for strongly coupled phases. In *Numerical Methods in Multiphase Flows 1994, ASME Fluids Engineering Division Summer Meeting, Lake Tahoe, U.S.A.FED-Vol 185,191-202*, 1994.

[15] J. Lavieville, E. Deutsch, and O. Simonin. Large eddy simulation of interactions between colliding particles and a homogeneous isotropic turbulence field. *Gas-Particle Flows,ASME,FED*, 228:359–369, 1995.

[16] PCB piezotronics Inc. *Product catalogue.*

[17] M. A. Rizk and S. E. Elgobashi. A two equation turbulence model for dispersed dilute confined two-phase flow. *Int.J.Multiphase Flow*, 15:119–133, 1989.

[18] L.A. Rosendahl. *Extending the modelling framework for gas particle systems: Applications of multiparameter shape descriptions to non-conventional solid fuels in reacting and non-reacting environments.* PhD thesis, Aalborg University, Institute of Energy Technology, 1998.

[19] H. Schlichting and K. Gersten. *Boundary Layer Theory.* Springer-Verlag, New York, 2000.

[20] M. Sommerfeld and G. Zivkovic. *Comput. Methods Appl.Sci.* Number 201. 1992.

[21] O. Triesch and M. Bohnet. Measurement and CFD prediction of velocity and concentration profiles in a decelerated gas-solids flow. *Powder Technology*, 115(2):101–113, 2001.